

# CO<sub>2</sub> Dissociative Sticking on Cu(110)

## CO<sub>2</sub> Dissociative Sticking on Cu(110)

Federico J. Gonzalez,<sup>1</sup> Carmen A. Tachino,<sup>1,2</sup> and H. Fabio Busnengo<sup>1,2</sup>

<sup>1)</sup>*Grupo de Fisicoquímica en Interfaces y Nanoestructuras,*

*Instituto de Física Rosario (IFIR), CONICET-UNR, Bv. 27 de Febrero 210 bis,*

*S2000EKF Rosario, Argentina*

<sup>2)</sup>*Facultad de Ciencias Exactas, Ingeniería y Agrimensura,*

*Universidad Nacional de Rosario, Av. Pellegrini 250, S2000 Rosario,*

*Argentina*

(\*Corresponding author: busnengo@ifir-conicet.gov.ar)

(Dated: 29 December 2025)

## CO<sub>2</sub> Dissociative Sticking on Cu(110)

In this work we investigate the dissociation of CO<sub>2</sub> on Cu(110) by performing density functional theory calculations using the vdW-DF2 exchange-correlation functional. The total energies obtained were employed to parameterize an artificial neural network potential energy surface by using an active learning iterative approach. The obtained potential was then used in quasi-classical trajectory calculations of molecular and dissociative adsorption probabilities as a function of the initial impact energy of the molecules and surface temperature. We compare our results with available supersonic molecular beam experimental data for normal incidence. Concerning the general dependence of the molecular and dissociative adsorption probabilities on the initial translational energy of the molecules, our theoretical results agree with experiments. Also in agreement with experiments we have found that dissociative adsorption is not affected by surface temperature between 50 K and 400 K, for impact energies for which the dissociation probability is larger than  $\sim 10^{-3}$ . We have investigated the influence of impact energy and surface temperature on the final state of the dissociation products by extending the time integration of the reactive trajectories up to 10 ps. We have found that above  $\sim 2.5$  eV and close to or above room temperature, CO<sub>2</sub> dissociation induces strong surface distortions including final structures involving Cu adatoms. The creation of Cu vacancy-adatom pairs is stimulated by the presence of both CO<sub>ads</sub> and O<sub>ads</sub> which interact strongly with the Cu adatoms and even give rise to unexpected (O-Cu-CO)<sub>ads</sub> linear moieties anchored to the surface by the dissociated O atom and involving a Cu adatom almost detached from the surface. These surface distortions produced by dissociation products of high energy CO<sub>2</sub> molecules at and above room temperature might explain recent experiments that have found a saturation oxygen coverage for high energy molecules, larger than for slow molecules.

## I. INTRODUCTION

The interaction of CO<sub>2</sub> with copper surfaces has attracted considerable attention due to the application of Cu-based catalysts in the conversion of CO<sub>2</sub> to value-added products, such as methanol, ethanol, and other C<sub>1</sub> and C<sub>2+</sub> compounds<sup>1–3</sup>. A fundamental challenge in this process is the activation of CO<sub>2</sub> due to its high stability<sup>4,5</sup>. Though the most efficient Cu-based catalysts for CO<sub>2</sub> conversion consist of Cu particles deposited on oxide supports<sup>6,7</sup>, understanding in detail the way CO<sub>2</sub> interacts and adsorbs on simpler systems such as flat Cu surfaces is also of great interest. Whether CO<sub>2</sub> dissociates or not upon adsorption on Cu(110) (the most active low-Miller-index face of copper<sup>8</sup>) has been a subject of debate. Early ultra-high vacuum (UHV) experimental studies found that low energy CO<sub>2</sub> molecules do not chemisorb on Cu(110) and the estimated energy barrier (E<sub>b</sub>) for dissociation was 0.69 eV<sup>9,10</sup>. However, experiments conducted by Funk *et al.* with supersonic molecular beams (SMB) were unable to detect dissociation events for incidence energies E<sub>i</sub> up to 1.3 eV (i.e. almost twice the value of the estimated energy barrier), and only molecular adsorption was observed at low surface temperatures, T<sub>s</sub> ∼ 90 K<sup>11</sup>.

Recent SMB studies by Singh and Shirhatti have shed new light on these apparently contradicting results<sup>12</sup>. They measured initial dissociative sticking probabilities, S<sub>0</sub>, varying from ∼ 3 × 10<sup>−4</sup> for E<sub>i</sub>=0.65 eV to ∼ 2 × 10<sup>−2</sup> for E<sub>i</sub>=1.59 eV. Thus, in spite of observing dissociation events at relatively low impact energies, these results are not in contradiction with those of Funk *et al.* who would have not observed signs of CO<sub>2</sub> dissociation due to the detection limit of their experiments (∼ 0.03). In addition, based on their results and extrapolations to higher impact energies through considerations based on a low-dimensional description of the CO<sub>2</sub> dissociation dynamics, Singh and Shirhatti estimated the energy barrier for CO<sub>2</sub> dissociation to be E<sub>b</sub> ∼ 2 eV<sup>12</sup>, in strong contrast with density functional theory (DFT) results that predict an energy barrier E<sub>b</sub>=0.64 eV<sup>13,14</sup>. Motivated by the latter work, Yin and Guo performed full dimensional quasi-classical trajectory (QCT) calculations using an artificial neural network potential energy surface (ANN-PES) based on DFT calculations (with the optPBE-vdW functional<sup>15</sup>) and obtained dissociative adsorption probabilities, P<sub>diss</sub>, smaller than 1.5 × 10<sup>−2</sup> even for an impact energy more than three times higher than the lowest energy barrier for dissociation of their ANN-PES, E<sub>b</sub>=0.63 eV. Thus, they showed that the low reactivity of Cu(110) found in experiments for CO<sub>2</sub> is not only due to a relatively large energy barrier for dissociation but also to the tight character of the transition state and the complexity of the high-dimensional molecule-surface CO<sub>2</sub>/Cu(110) interaction

## CO<sub>2</sub> Dissociative Sticking on Cu(110)

dynamics<sup>16</sup>.

In a recent attempt to extend the impact energy range of their previous SMB experiments, Singh and Shirhatti performed new measurements for E<sub>i</sub> up to 4.6 eV<sup>17</sup>. In contrast with the rapid increase of P<sub>diss</sub>(E<sub>i</sub>) observed at lower energies, for E<sub>i</sub> > 3 eV P<sub>diss</sub> tends to level off at a value  $\sim 4.1 \times 10^{-2}$ , increasing only by a factor 1.5 in the wide 2.0–4.6 eV E<sub>i</sub>-range. Furthermore, they also found that the O atom saturation coverage obtained for large exposures of CO<sub>2</sub> molecules with E<sub>i</sub>  $\gtrsim$  3 eV, is larger than for lower impact energy molecules (0.66 ML vs. 0.5 ML). This might indicate that for molecules with E<sub>i</sub> higher than 3 eV, there are final states of the dissociation products not accessible at lower impact energies, but this has not yet been elucidated experimentally.

In this work we revisit the dynamics of CO<sub>2</sub> dissociation on Cu(110) through QCT calculations based on an ANN-PES parameterized from DFT total energies obtained using the vdW-DF2 exchange-correlation functional<sup>18</sup> used previously with success for CO/Cu(110)<sup>19,20</sup>. We focus our study on the dynamics of the CO<sub>2</sub> molecules with impact energies in the whole E<sub>i</sub>-range investigated in Refs. 12,17. We analyze in detail all the possible final states of the molecule, for molecular and dissociative adsorption. In particular, we investigate and quantify to what extent the impact energy and surface temperature influence the final state of the dissociation products, including the generation of surface defects.

## II. METHODOLOGY

### A. DFT Calculations

Total energies for the CO<sub>2</sub>/Cu(110) system were computed using the nonlocal van der Waals density functional vdW-DF2, originally proposed by Lee *et al.*<sup>18</sup>, to account for dispersion interactions. We have used the Vienna ab initio simulation package (VASP)<sup>21–26</sup>, which employs a plane-wave basis set to represent electronic wavefunctions and accounts for electron-ion interactions through the projector augmented-wave (PAW) method<sup>27</sup>. The cutoff energy for plane wave expansions was set at 450 eV, and the Methfessel–Paxton scheme<sup>28</sup> was used with a smearing width of 0.4 eV. The Cu(110) surface was modeled as a five-layer slab substrate with a vacuum of 13.6 Å in the direction normal to the surface. The Cu atoms in the two bottom layers were kept fixed with the ideal inter-layer distance between consecutive 110 planes in bulk,  $a_{Cu}\sqrt{2}/4$ , with  $a_{Cu}$  being the obtained optimum theoretical lattice constant,  $a_{Cu}=3.754$  Å. In contrast, the posi-

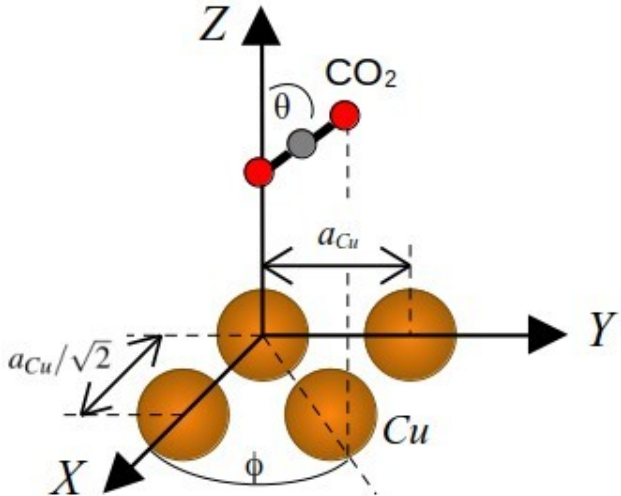


FIG. 1. Schematic representation of the CO<sub>2</sub> molecule in its equilibrium configuration far from the surface, and coordinate system used throughout this work. Z=0 corresponds to the plane containing the outermost-layer Cu atoms, in the lowest-energy clean surface structure. High symmetry sites: top (X=0, Y=0); short-bridge (X=a<sub>Cu</sub>/(2 $\sqrt{2}$ ), Y=0); long-bridge (X=0, Y=a<sub>Cu</sub>/2); hollow (X=a<sub>Cu</sub>/(2 $\sqrt{2}$ ), Y=a<sub>Cu</sub>/2).

tions of the Cu atoms in the three topmost layers of the Cu(110) slab were optimized to account for the relaxation of the clean surface and also in geometry optimizations of adsorbate/surface structures. We performed DFT calculations for (3×2) and (3×3) supercells using 7×7×1 and 7×5×1 Monkhorst–Pack  $\mathbf{k}$ -point grids<sup>29</sup> respectively. In general, the DFT calculations were spin restricted except for those configurations with the O atom far from the surface for which we performed spin-polarized calculations. All these settings of the DFT calculations are consistent with those used previously in Ref. 19 to deal with CO/Cu(110).

All geometry optimizations were performed until the forces acting on all mobile atoms were smaller than 0.1 eV/Å. The reported optimum geometry of CO<sub>2</sub> in vacuum was actually obtained in calculations with the molecule in the middle of the  $\sim 13.6$  Å vacuum space left between the slab and its closest periodic images. The equilibrium C–O bond lengths found for the optimum linear configuration of CO<sub>2</sub> are both 1.177 Å. The CO<sub>2</sub> molecule in its equilibrium configuration far from the surface is shown in Fig. 1 where we also illustrate the system coordinate used along this work. The minimum energy pathways (MEP) for all the reactive processes we have investigated were computed using the nudged elastic band (NEB)<sup>30–32</sup> and dimer<sup>33</sup> methods. The character of true saddle point of the PES for all the transition states (TS) reported in this work was confirmed by checking the existence of only one negative eigenvalue of the Hessian matrix of the DFT-PES.

## B. The ANN-PES

From the DFT total energies for a large set of configurations of the CO<sub>2</sub>/Cu(110) system, we developed a PES using the atomistic neural network (ANN) method implemented in the atomic energy network (`ænet`) code<sup>34–36</sup>. Using this method, the total energy of the system, E<sub>ANN</sub>, is expressed as the sum of a chemical-environment-dependent energy of each atom in the supercell (considering periodic boundary conditions):

$$E_{ANN} = \sum_{\alpha=1}^{N_{type}} \sum_{i=1}^{N_{\alpha}} E_i^{(\alpha)}, \quad (1)$$

where E<sub>i</sub><sup>(α)</sup> is the energy of the *i*<sup>th</sup> atom of species  $\alpha$  ( $\alpha$ =Cu, C, O), N<sub>type</sub> is the number of atomic species, and N<sub>α</sub> is the number of atoms of species  $\alpha$ . The chemical environment of each atom was described using the radial (G<sup>2</sup>) and angular (G<sup>4</sup>) descriptors introduced by Behler and Parrinello (see Ref. 37 and references therein) as we have successfully used for CO/Cu(110)<sup>19</sup>. For the atoms of the three species, E<sub>i</sub><sup>(α)</sup> was computed using a feed-forward neural network with two hidden layers and 10 neurons per layer, and the hyperbolic tangent as activation function.

For the G<sup>2</sup> and G<sup>4</sup> symmetry functions involving pairs and triads of species necessary to describe the system CO/Cu(110), here we have used the same parameters as in Ref. 19. For CO<sub>2</sub>/Cu(110) one extra O-O radial function, and four extra angular functions (Cu-O-O, C-O-O, O-Cu-O, and O-C-O) are needed due to the extra O atom. For the O-O radial function, we have used:  $\eta=0.05, 0.23, 1.07, 2.0$  with R<sub>s</sub>=0.0 and R<sub>c</sub>=7.0 Å, whereas for the four extra angular symmetry functions we have used:  $\eta = 0.05$ ,  $\lambda = \{-1, 1\}$ ,  $\zeta = \{1, 4\}$  and R<sub>c</sub>=7.0 Å.

In order to optimize the ANN-PES for CO<sub>2</sub>/Cu(110) we have used an active learning approach. We have started with an initial database of configurations whose DFT total energies are used to minimize the root mean square error (RMSE) of the energies predicted by five ANN-PESs:

$$RMSE = \left[ \frac{1}{N_{conf}} \sum_{j=1}^{N_{conf}} (E_{DFT,j} - E_{ANN,j})^2 \right]^{1/2}, \quad (2)$$

where N<sub>conf</sub> is the number of configurations in the database, and E<sub>DFT,j</sub> and E<sub>ANN,j</sub> are the DFT total energy and the ANN-PES value for the *j*<sup>th</sup> configuration respectively. Actually, only 90% of the configurations in the database have been used for training because 10% of the configurations were selected (randomly) for testing, in order to detect signs of overfitting<sup>37</sup>. The five ANN-PESs differ with respect to each other only due to the different initial values of the weights and

## CO<sub>2</sub> Dissociative Sticking on Cu(110)

bias of the ANNs which are chosen randomly. Among the five initial ANN-PES, we selected the one with the lowest RMSE for the training and testing sub-sets of configurations, and used it to calculate MEPs for various process of interest (using the climbing image NEB, CI-NEB, method<sup>32,38–42</sup> as implemented in the ASE package<sup>43,44</sup>), and to perform quasi-classical trajectory (QCT) calculations for various impact energies of the impinging CO<sub>2</sub> molecules on Cu(110). From these calculations, we selected configurations to evaluate the energy using the five ANN-PESs. For each configuration we compute the maximum discrepancy between the values predicted by the five ANN-PESs, and for those whose largest discrepancy exceeded 0.05 eV, we performed a DFT total energy evaluation and incorporated the configuration to the database.

The initial database for CO<sub>2</sub>/Cu(110) included the full database of 7 803 configurations used to parameterize the ANN-PES for CO/Cu(110) employed in Refs. 19,20, plus extra configurations of CO<sub>2</sub>/Cu(110), (CO+O)/Cu(110) (dissociated states) and also a few for Cu(110) using two supercells: (3×2) and (3×3). The great majority of these extra configurations correspond to:

- (i) CO<sub>2</sub> in its equilibrium geometry, and vibrating in its different normal modes (asymmetric stretching, AS, symmetric stretching, SS, and bending, B) far from the surface,
- (ii) CO<sub>2</sub> in its equilibrium geometry on the four highest symmetry surface sites of Cu(110) (i.e. top, short-bridge, long-bridge and hollow), parallel and perpendicular to the surface at different heights of the center of mass of the molecule above the outermost-layer Cu atoms which are kept fixed in their equilibrium positions. The results of these calculations are shown in Fig. 2,
- (iii) idem to (ii) but with the C–O bond lengths changed with respect to the equilibrium value by  $\pm 0.1$ ,  $0.2$  Å (consistent with vibrations in the AS and the SS mode), and with angles between the two C–O bonds of 140, 145, 150, 155, 160, 165, 170, 175, and 180 deg,
- (iv) CO<sub>2</sub>/Cu(110) evaluated using DFT calculations while looking for local minima of the PES corresponding to possible final states of CO and O after dissociation (close and far from each other), the optimum geometry of physisorbed states, and the bent molecularly chemisorbed state reported in the literature<sup>16</sup>,
- (v) images of DFT-based-NEB calculations explored while looking for MEPs and transition states (TS) from a physisorbed to the chemisorbed bent state (TS1), and from a physisorbed to the dissociated state (TS2), and

## CO<sub>2</sub> Dissociative Sticking on Cu(110)

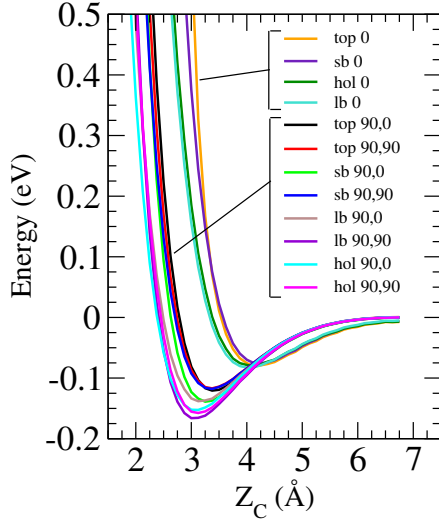


FIG. 2. DFT-vdW-DF2 total energy of CO<sub>2</sub> in its equilibrium geometry in vacuum, as a function of the molecule surface distance measured by the Z coordinate of the C atom above the outermost-layer of surface atoms which are kept fixed in their equilibrium positions. Each line corresponds to a different surface high symmetry site: top, short-bridge (sb), long-bridge (lb), and hollow (hol) and/or a different orientation as indicated in the inset by the values of the polar and azimuthal angles of the molecule. For instance, hol 90,0 (lb 0) indicates that the center of mass of the molecule is on a hollow (long-bridge) site and the polar and azimuthal angles of (the polar angle of) the molecular axis containing the two C–O bonds are 90 deg and 0 deg respectively (is 0 deg).

(vi) (O+CO)/Cu(110) for CO fixed on top of Cu atom in its optimum chemisorption configuration, and the O atom on the high-symmetry surface sites (near and far from CO), with its Z coordinate (measured with respect to the outermost-layer Cu atoms), Z<sub>0</sub>, varying from 0 to 6.8 Å and with O in the positions visited by the DFT geometry optimization performed looking for local minima of the PES.

During the iterative active learning method, we applied a descriptor-based filter to the database to avoid redundant-information (too similar) configurations (characterized by discrepancies between all the descriptors <0.5% and energy differences <5 meV). The active-learning loop was repeated ten times until obtaining stable predictions with the resulting ANN-PES, in particular for the geometry and energy of relevant intermediate, final (dissociated) and transition states, as well as for the dissociative adsorption probability (P<sub>diss</sub>) at different impact energies. At the end, the final database consists of 81 657 configurations with energies computed using DFT calculations.

### C. QCT calculations

QCT calculations were performed for initially non-rotating CO<sub>2</sub> molecules impinging on Cu(110) at normal incidence. We employed the gas-surface reaction dynamics (GSRD) code developed in our group, which has been previously used to investigate scattering and adsorption for various molecule/surface systems using Tersoff-like reactive force fields (RFF)<sup>45–49</sup> and more recently also with ANN-PESs<sup>19,50</sup>. This code integrates the equation of motion of the system using the direct Beeman method<sup>51</sup>, a variant of the Verlet integration algorithm<sup>52,53</sup>. As mentioned in the previous section, these calculations were performed not only to compute observables in production stage but also during the iterative optimization of the ANN-PES.

Once the final version of the ANN-PES was obtained, for each initial condition corresponding to a molecular impact energy  $E_i$  ranging between 0.01 eV and 4.5 eV and a surface temperature  $T_s$  between 50 K and 400 K, we have integrated 10 000 trajectories with a maximum propagation time of  $t_{\text{sup}}=100$  ps and a time step of 0.5 fs. For each trajectory, the initial positions and velocities of the Cu atoms were randomly selected from a large set of *snapshots* generated previously during a long NVT simulation for the clean surface at the  $T_s$  value of interest, controlled through a Berendsen thermostat<sup>54</sup>.

In order to simulate initially non-rotating CO<sub>2</sub> molecules in the vibrational ground state (GS) and in vibrationally excited states of the asymmetric stretching (AS), symmetric stretching (SS), and bend (B) modes, the initial coordinates and velocities of their C and O atoms (with respect to the molecular CM) were selected following the standard procedure detailed in reference<sup>55</sup>, and selecting randomly the molecular orientation. Then, the CO<sub>2</sub> center of mass (CM) was initially positioned at a distance of 8.5 Å above the topmost-layer of the Cu(110) surface ( $Z_{\text{CM}}=8.5$  Å) and the lateral coordinates,  $X_{\text{CM}}$  and  $Y_{\text{CM}}$ , were uniformly sampled randomly within the whole simulation supercell. Finally, the desired initial velocity of the molecular CM directed perpendicularly towards the surface for normal incidence conditions was added to all the atoms of the molecule.

In the QCT calculations we have considered as reflected to those molecules for which, after interacting with the surface, the Z coordinate of the CM reaches a value larger than in the initial state, i.e.  $Z_{\text{CM}} > 8.5$  Å and the CM momentum vector points toward the vacuum. Whenever this condition is fulfilled, we stopped the integration of the trajectory and the time is considered as its *reflection time*. On the other hand, we have considered that a dissociative adsorption event has taken place whenever one of the two C–O bonds reaches a length equal to 1.8 Å and we define

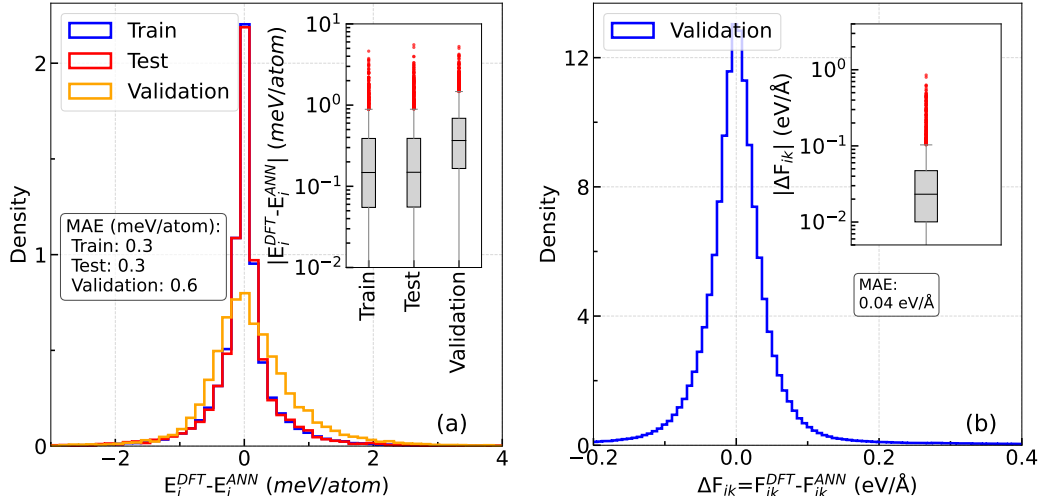


FIG. 3. (a) Histogram of energy differences ( $E_{DFT} - E_{NN}$ ) for the training, test, and validation sets. (b) Force prediction errors for the validation set.

that time as *dissociation time*. However, in this case we have continued the integration of the trajectories up to 10 ps in order to characterize better the *final state* of the dissociation products (allowing molecule-surface energy exchange and dissipation during several picoseconds after the dissociation time). Finally, for those trajectories for which none of the two conditions mentioned above is fulfilled at a time  $t = t_{\text{sup}} = 100$  ps, we consider that the molecule has been molecularly adsorbed. Accordingly, we define reflection, dissociative adsorption, and molecular adsorption probabilities ( $P_{\text{ref}}$ ,  $P_{\text{diss}}$ , and  $P_{\text{molads}}$ , respectively) as the ratio of the number of trajectories that fulfill the corresponding final condition and the total number of trajectories integrated for a given initial condition defined by the impact energy and vibrational state of the molecule and the surface temperature.

### III. RESULTS AND DISCUSSIONS

#### A. ANN-PES validation

As already mentioned in section II B, 90% of the configurations of the total database were used for training (training set) and the other 10% were used for testing (testing set). In addition, during the training process we have selected a set of 12 675 configurations from the QCT calculations, whose total energy was evaluated using DFT but they were not incorporated to the database, in

order to use them for validation (validation set).

Fig. 3(a) shows the histograms of energy errors per atom (E<sub>DFT</sub>-E<sub>ANN</sub>) for the training, testing and validation sets of configurations. It can be seen that most of the values are in the interval from -2 to 2 meV/atom. Within the figure we also report the mean absolute error (MAE) per atom for the energy,

$$\text{MAE}_E = \frac{1}{N_{\text{conf}}} \sum_{j=1}^{N_{\text{conf}}} \frac{1}{N_{\text{atom},j}} |E_{DFT,j} - E_{ANN,j}|, \quad (3)$$

with N<sub>conf</sub> being the number of configurations in the corresponding set, and N<sub>atom,j</sub> the number of atoms in the *j*<sup>th</sup> configuration. In addition, in the inset we show the boxplots (as implemented in matplotlib<sup>56</sup>) of the absolute errors for the three sets of configurations. They show that 50% (75%) of the configurations in the training, testing and validation sets have absolute errors smaller than 0.15, 0.15 and 0.37 meV/atom (0.39, 0.39, and 0.69 meV/atom) respectively. These similar and small absolute errors obtained for the three sets of data is a strong indication that our model is not overfitted. There are some outlier configurations (represented by red symbols) with absolute errors up to  $\sim$  8 meV/atom, but they represent only the  $\sim$  6.6% of the configurations and it is not expected they could produce significant artifacts in the dynamics.

To quantify the errors in the forces predicted with the ANN-PES with respect to the DFT values, we have also computed the MAE for the forces using the expression:

$$\text{MAE}_F = \frac{1}{N_{\text{conf}}} \sum_{j=1}^{N_{\text{conf}}} \sum_{k=1}^{N_{\text{atom},j}} \frac{1}{N_{\text{atom},j}} \sum_{\alpha} |F_{DFT,jk\alpha} - F_{ANN,jk\alpha}|, \quad (4)$$

where F<sub>ANN,jk $\alpha$</sub>  (F<sub>DFT,jk $\alpha$</sub> ) is the  $\alpha$ -component ( $\alpha = x, y, z$ ) of the ANN-PES (DFT) force acting on the *k*<sup>th</sup> atom of the *j*<sup>th</sup> configuration. For the validation set (characterized by larger errors than the training and testing ones) we obtained MAE<sub>F</sub>=0.04 eV/Å. Fig. 3(b) shows the histogram for the errors in the forces  $\Delta F_{jk}$  for the validation set. It is observed that the great majority of them lie between -0.2 and 0.2 eV/Å. In the inset we also show the boxplot for the validation set which exhibits a relatively small set of outliers with errors from 0.1 to 1 eV/Å.

It is important to mention that during the last steps of the iterative active learning procedure, the values of P<sub>diss</sub> for various impact energies differ by no more than a few percent with respect to the values predicted with the final ANN-PES which indicates a good convergence of our procedure with respect to the observable of most interest for this work. In addition, we have found that using the present ANN-PES developed for CO<sub>2</sub>/Cu(110), the molecular adsorption probabilities for CO/Cu(110) under normal incidence differ by less than 2% with respect to the values reported

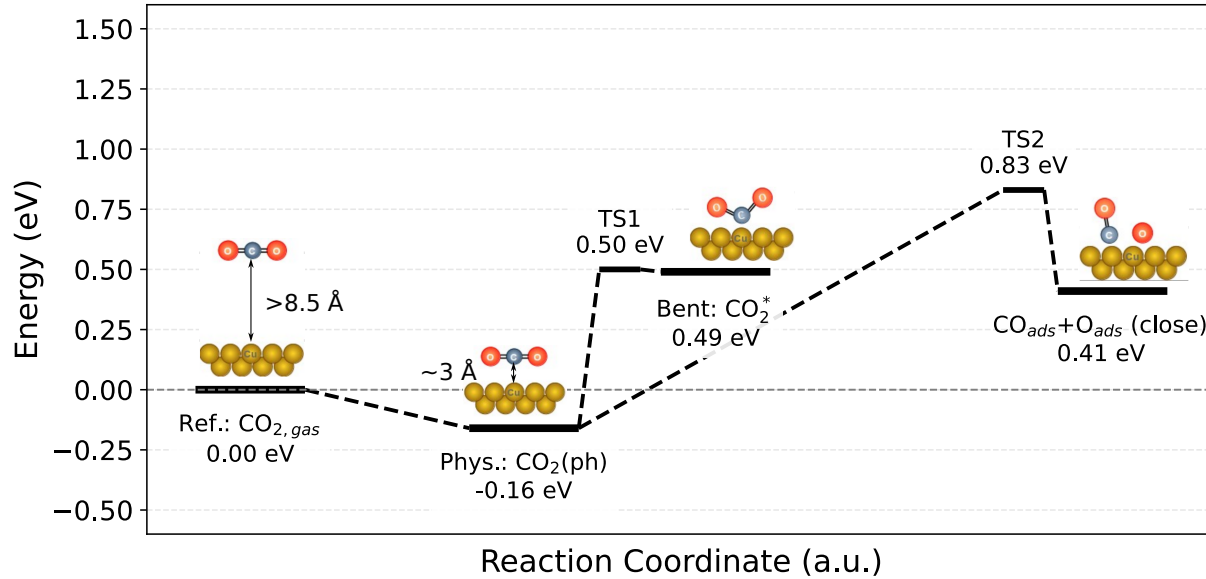


FIG. 4. Energetics of CO<sub>2</sub> physisorption, molecular chemisorption and dissociation on Cu(110), including the involved local minima and transition states found along minimum energy pathways connecting them.

in Ref. 19.

To further validate the accuracy of the ANN-PES, we use it for a systematic exploration of the CO<sub>2</sub>/Cu(110) potential energy landscape including determination of local minima and minimum energy pathways for molecular and dissociative adsorption, as well as diffusion of the dissociation products. The most relevant configurations found in these calculations were then evaluated using DFT and we have obtained discrepancies not larger than 30 meV.

## B. Characterization of the CO<sub>2</sub>/Cu(110) ANN-PES

By exploring the properties of the ANN-PES of CO<sub>2</sub>/Cu(110) relevant for dissociative adsorption, we have identified four local minima corresponding to: (i) both the CO<sub>2</sub> molecule and the surface in their equilibrium configurations when they are from each other, CO<sub>2,gas</sub>; (ii) the physisorbed state of CO<sub>2</sub>, CO<sub>2(ph)</sub>; (iii) a chemisorbed bent configuration of CO<sub>2</sub>, CO<sub>2\*</sub>; and (iv) the dissociated state, CO<sub>ads</sub>+O<sub>ads</sub>, with the two dissociation products close to each other (within the same surface unit cell). The energy of these four local minima (taking CO<sub>2,gas</sub> as the reference zero-energy configuration) and the transition states along the minimum energy pathways (MEP)

## CO<sub>2</sub> Dissociative Sticking on Cu(110)

connecting them are shown in Fig. 4.

Physisorption is a non-activated process and there is no energy barrier along the MEP connecting the CO<sub>2</sub>(g) and CO<sub>2</sub>(ph) states. CO<sub>2</sub>(ph) corresponds to a weakly bound molecular configuration due to the van der Waals interaction with Cu(110). In this configuration the molecule is located parallel to the surface (with its equilibrium geometry barely changed with respect to vacuum) with the Z coordinate of its center of mass, Z<sub>CM</sub>  $\sim$  3 Å. The energy of this physisorbed state is -0.16 eV which is consistent with the value previously reported using the same vdW-DF2 functional<sup>57</sup> but corresponds to a desorption energy slightly smaller than the value extracted from temperature programmed desorption (TPD) experiments<sup>58</sup>. This state is the global minimum of the CO<sub>2</sub>/Cu(110) PES. Fig. 2 indicates that physisorbed molecules can diffuse over the surface by overcoming an energy barrier  $\sim$  0.05 eV.

The dissociated state with CO and O adsorbed within the same surface unit cell (with CO on top of a Cu atom and O occupying a pseudo three-fold adsorption site forming bonds with two nearest neighbor outermost-layer Cu atoms and a Cu atom in the second surface layer) has the energy +0.41 eV. Finally, we have also found a bent chemisorbed state that exhibits a tridentate molecular configuration with each atom of the molecule bound to a different Cu atom of the surface unit cell and the angle O–C–O being  $\sim$  123 deg. Such a bent configuration is usually associated with a partial charge transfer from the surface to the antibonding  $\pi^*$  orbitals of CO<sub>2</sub>, thereby facilitating its activation toward dissociation or reduction<sup>59</sup>. The obtained optimum geometry of this bent-CO<sub>2</sub><sup>\*</sup> state is very similar to the one reported previously characterized by a O–C–O angle between 120 deg and 140 deg<sup>16,60</sup>. However, its energy (i.e. 0.49 eV) is significantly higher than the value obtained by Yin and Guo (i.e. 0.06 eV) which is very likely due to the use of different XC functionals (vdW-DF2 used here vs. optPBE-vdW used in Ref. 16).

In Fig. 4 we also show the energies of two transition states along the MEPs connecting the physisorbed state with the bent-CO<sub>2</sub><sup>\*</sup> state (TS1) and with the dissociated state (TS2). The energies of TS1 and TS2 (with respect to CO<sub>2,gas</sub>) are 0.50 eV and 0.83 eV respectively. The optimum geometry (Fig. 5) and the energy of the TS2 structure (with respect to that of CO<sub>2</sub>(ph)) obtained with our ANN-PES are very close to that of the transition state (also called TS2) reported by Yin and Guo<sup>16</sup> using the optPBE-vdW functional (0.99 eV vs. 0.87 eV). The energy barrier to escape from the bent-CO<sub>2</sub><sup>\*</sup> state towards the CO<sub>2</sub>(ph) state is only 0.01 eV. This entails a very small stability of the bent chemisorbed state. The corresponding energy barrier reported by Yin and Guo is also small (0.08 eV) but still larger than ours by 0.07 eV<sup>16</sup>. This small stability predicted for the

## CO<sub>2</sub> Dissociative Sticking on Cu(110)

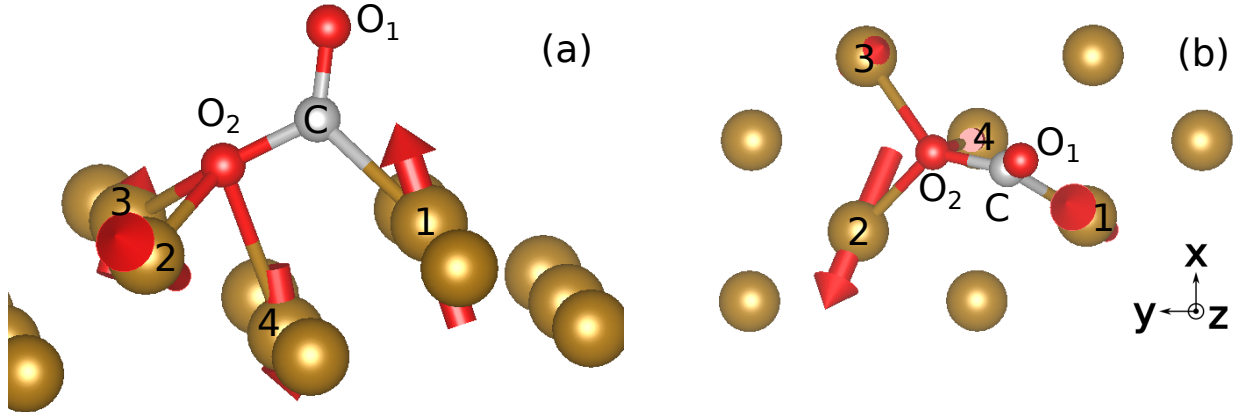


FIG. 5. (a) Top view, and (b) side view of the transition state TS2 along the minimum energy pathway for CO<sub>2</sub> dissociation on Cu(110), connecting the physisorbed and the most stable dissociated state. Dark and light orange distinguish topmost-layer and second-layer Cu atoms respectively. Relevant distances/coordinates:  $d(C-O_1)=1.39$  Å,  $d(C-O_2)=1.21$  Å,  $Z_{CM}=1.58$  Å,  $d(C-Cu_1)=2.05$  Å,  $d(O_2-Cu_2)=2.02$  Å,  $d(O_2-Cu_3)=2.13$  Å,  $d(O_2-Cu_4)=2.45$  Å. In (a) the red arrows represent the displacements of Cu atoms (larger than 0.1 Å) with respect their positions in the reference configuration (see the text) of lengths: 0.23 Å, 0.24 Å, 0.33 Å, and 0.15 Å for the Cu atoms labeled as 1, 2, 3, and 4 respectively.

CO<sub>2</sub><sup>\*</sup> state is consistent with the results of the experimental investigations that have not been able to detect a bent chemisorbed state of CO<sub>2</sub> on the (110) face of copper<sup>10,58</sup>.

It must be mentioned that we have also tried to compute a MEP connecting directly the bent-CO<sub>2</sub><sup>\*</sup> state with the dissociated state (i.e. not passing through CO<sub>2</sub>(ph)) but in spite of many attempts through NEB calculations with different settings, we did not succeed. All the obtained dissociation pathways starting from bent-CO<sub>2</sub><sup>\*</sup>, passed first by a more stable physisorbed state and the energy barriers obtained were always very close to that of TS2 reported in Figs. 4 and 5.

Before concluding this section it is important to emphasize that the energy of all the relevant configurations displayed in Fig. 4 were evaluated with DFT calculations. The obtained discrepancies with respect to the ANN-PES values were always smaller than 0.03 eV. Moreover, DFT calculations confirmed the local minimum or saddle point character predicted by the ANN-PES for all these configurations. This provides strong support for the use of the ANN-PES for large-scale dynamical simulations of CO<sub>2</sub> scattering, adsorption and dissociation on Cu(110).

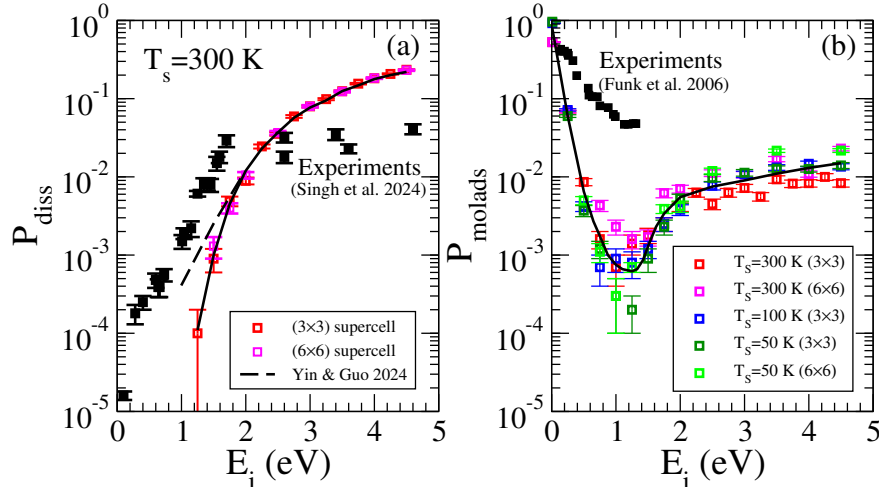


FIG. 6. (a)  $P_{\text{diss}}$  as a function of the impact energy,  $E_i$ , for normal incidence and  $T_s=300$  K. Full black squares, experimental data taken from Refs. 12,17. Red open squares, QCT results for a  $(3 \times 3)$  supercell (present work), magenta open squares, QCT results for a  $(6 \times 6)$  supercell (present work). Dashed black line, QCT results taken from Ref. 16. (b)  $P_{\text{molads}}$  as a function of the impact energy,  $E_i$ , for normal incidence. Full black squares, experimental data taken from Ref. 11. Open squares, QCT results (present work) for different surface temperatures and supercells: red, 300 K and  $(3 \times 3)$ ; magenta, 300 K and  $(6 \times 6)$ ; blue, 100 K and  $(3 \times 3)$ ; dark green, 50 K and  $(3 \times 3)$ ; light green, 50 K and  $(6 \times 6)$ . The full black lines in both panels are plotted to guide the eyes.

### C. QCT results

In Fig. 6(a) we show the dissociative sticking probability,  $P_{\text{diss}}$ , of CO<sub>2</sub> on Cu(110) as a function of the initial translational energy of the molecules,  $E_i$ , under normal incidence, compared with available supersonic molecular beam experimental data for a surface temperature  $T_s=300$  K<sup>12,17</sup>. Our QCT results (for CO<sub>2</sub> initially in its roto-vibrational ground state) are also compared with those reported recently by Yin and Guo<sup>16</sup>, obtained using a similar methodology. We have considered two supercells:  $(3 \times 3)$  (as used by Yin and Guo<sup>16</sup>) and  $(6 \times 6)$ . Fig. 6(a) shows that the values of  $P_{\text{diss}}$  obtained with both supercells are very close to each other.

As expected for activated dissociative adsorption,  $P_{\text{diss}}$  shows a monotonic increasing  $E_i$ -dependence in qualitative agreement with the supersonic molecular beam data. However, compared with experiments our results are too low for  $E_i \lesssim 2$  eV and too high for  $E_i \gtrsim 2$  eV. On the other hand, for  $E_i \lesssim 1.75$  eV our results are also smaller than those of Yin and Guo, which is very

## CO<sub>2</sub> Dissociative Sticking on Cu(110)

likely due to the higher minimum energy barrier (MEB) for CO<sub>2</sub> dissociation of our ANN-PES: 0.83 eV vs. 0.63 eV reported in Ref. 16. However, both theoretical results approach each other for higher values of  $E_i$ , suggesting that for such high impact energies,  $P_{\text{diss}}$  becomes much less sensitive to the value of the MEB. This is not surprising since for impact energies well above the MEB, dissociation can take place through an increasing number of reaction pathways, many of them not necessarily close to the MEP.

Above  $E_i \sim 2$  eV the experimental dissociative sticking probability becomes  $E_i$ -insensitive in contrast with our theoretical results, though in this high-energy range the slope of the theoretical  $P_{\text{diss}}(E_i)$  curve is much smaller than at low impact energies. It is important to mention that above  $E_i \sim 3$  eV, in experiments an atomic oxygen saturation coverage higher than that found for lower impact energies was observed. This might be an indication that the final states accessible for the dissociating CO<sub>2</sub> molecules on Cu(110) change from low to high impact energies. This motivates our analysis of the time evolution of CO and O post-dissociation presented below.

For  $E_i \gtrsim 1$  eV, most of the impinging CO<sub>2</sub> molecules that do not dissociate are reflected back to vacuum. However, there is a non-negligible fraction of trajectories that remain (intact) near the surface even after a maximum integration time,  $t_{\text{sup}} = 100$  ps. The corresponding probability of molecular adsorption is here referred to as  $P_{\text{molads}}$ . Fig. 6(b) shows that no matter the size of supercell (3×3) or (6×6), and the surface temperature,  $P_{\text{molads}}$  presents a non-monotonic  $E_i$ -dependence.  $P_{\text{molads}}$  is very large for very low energies (varies between 0.5 and 1 depending on the considered value of  $T_s$ ), decreases with increasing  $E_i$  up to  $\sim 1.25$  eV, and then increases from its minimum value ( $\sim 10^{-3}$ – $10^{-4}$ ) and tend to level off close to  $10^{-2}$  for  $E_i \gtrsim 2.5$  eV. Thus, our calculations predict that molecular adsorption is the process with the highest probability at low impact energies ( $E_i \lesssim 0.1$  eV) and only for  $E_i \gtrsim 1.75$  eV,  $P_{\text{molads}}$  becomes smaller than  $P_{\text{diss}}$ . It might be argued that,  $P_{\text{molads}}$  values could change significantly with the size of the supercell employed in the calculations and  $T_s$ , because both factors are expected to affect the energy transfer from the molecule to the surface, necessary to stabilize high energy molecules near the surface. However, this is not the case. The results obtained for both (3×3) or (6×6) supercells, and different  $T_s$  values between 50 K and 300 K, lie all rather close to a single  $P_{\text{molads}}(E_i)$  curve (full black curve plotted to guide the eyes in Fig. 6(b)). For CO<sub>2</sub>/Cu(110), Funk *et al.* performed measurements of the trapping probability as a function of  $E_i$  at  $T_s=90$  K<sup>11</sup>, i.e. close below the desorption temperature of CO<sub>2</sub> observed in temperature programmed experiments<sup>58</sup>. The experimental molecular trapping probability is close to 0.4 at very low impact energies in reasonable agreement with our

## CO<sub>2</sub> Dissociative Sticking on Cu(110)

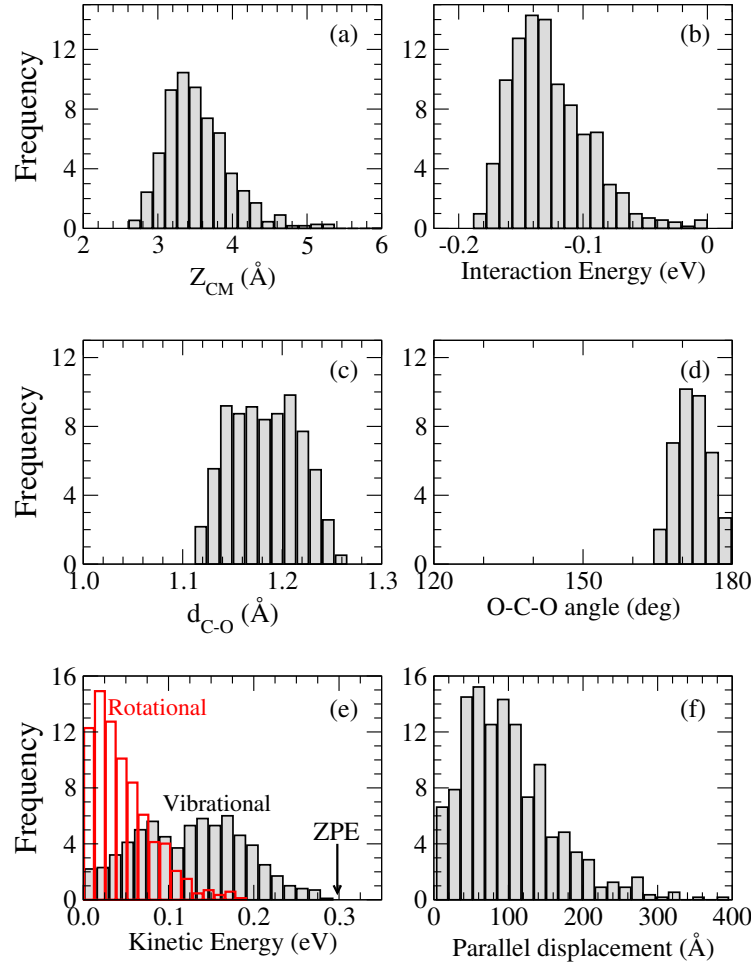


FIG. 7. Characterization of non-dissociated CO<sub>2</sub> molecules adsorbed at the final integration time of  $t_f=100$  ps. Results correspond to calculations made in a  $(6\times 6)$  supercell size, for normal incidence with initial kinetic energy  $E_i=0.25$  eV at a surface temperature  $T_s=300$  K. Distributions for: (a) final Z coordinate of the molecular center of mass,  $Z_{CM}$ . (b) final interaction energy (see main text for definition). (c) final C-O bond length,  $d_{C-O}$ . (d) final O-C-O bond angle. (e) final rotational (red histogram) and vibrational (grey histogram) kinetic energies. (f) Displacement of the molecular center of mass parallel to the surface.

results and also decreases (exponentially) with  $E_i$  but much less pronounced than the theoretical results. For instance, the theoretical  $P_{\text{molads}}$  values for  $E_i=1.25$  eV are smaller than the experiments by two orders of magnitude. The reason for such a big discrepancy is unclear to us, but it is highly unlikely due to a possible slight underestimation of the physisorption well-depth in our ANN-PES. In what follows, we will only present QCT results obtained using the  $(6\times 6)$  supercell

## CO<sub>2</sub> Dissociative Sticking on Cu(110)

except otherwise stated.

The analysis of the final state of low energy molecules that remain trapped near the surface at  $t_{\text{sup}}=100$  ps shows that they are all with  $Z_{\text{CM}}$  between 2.6 Å and 5.4 Å (see Fig. 7(a), for  $E_i=0.25$  eV and  $T_s=300$  K). The molecule-surface interaction energy defined as the difference between the potential energy of the configurations  $f$  and  $f'$ ,  $\Delta E=E_f-E_{f'}$  (with  $f$  being final configuration and  $f'$  is obtained from  $f$  by only translating rigidly the CO<sub>2</sub> molecule to a position where the interaction with the surface vanishes) is shown in Fig. 7(b). The obtained small and negative  $\Delta E$  values are consistent with the weak attractive molecule-surface interaction near the physisorption well shown in Fig. 2. In addition, the distributions of the C-O distances (Fig. 7(c)) are close to the equilibrium value for CO<sub>2</sub> in vacuum, and that of the O-C-O angle between the two C-O bonds differ from 180 deg by less than 15 deg (Fig. 7(d)). All these results demonstrate that molecules remaining trapped near the surface at  $t_{\text{max}}=10$  ps are physisorbed on the surface. The distribution of kinetic energy corresponding to vibrational motion is consistent with the molecular ZPE=0.298 eV, whereas the distribution of rotational kinetic energy shows signs of moderate rotational excitation (Fig. 7(e)). Finally, it is interesting to mention that these physisorbed molecules that have been trapped near the surface as long as 100 ps have experienced very large displacements parallel to the surface with respect to the initial aiming point as shown in Fig. 7(f).

Comparing the values of  $P_{\text{diss}}$  and  $P_{\text{molads}}$  shown in panels (a) and (b) of Fig. 6 respectively, it should be noted that  $P_{\text{molads}}$  is larger than  $P_{\text{diss}}$  by a factor expected larger than  $10^5$  for  $E_i \lesssim 1$  eV, that decreases to a value  $\sim 1$  for  $E_i=1.5$  eV, whereas for  $E_i \gtrsim 1.75$  eV  $P_{\text{diss}}$  becomes bigger than  $P_{\text{molads}}$ . Therefore, if in experiments a non-vanishing (even small) fraction of physisorbed molecules traveling large distances parallel to the surface (as shown in Fig. 7(f) for  $E_i=0.25$  eV) might encounter defect sites (e.g. steps) offering lower-energy-barrier dissociation pathways, the observed dissociative adsorption probability at low impact energies might be significantly larger than the values predicted by our calculations for a defect-free Cu(110) model surface. However, quantifying the role of defects certainly requires further modeling<sup>61,62</sup> beyond the scope of this paper.

In the  $E_i$ -range in which  $P_{\text{diss}} > P_{\text{molads}}$  (i.e.  $E_i \geq 1.75$  eV), both dissociative sticking and reflection events take place with interaction times smaller than 0.6 ps and 1.2 ps respectively. This is illustrated by Fig. 8. In addition, it shows that for 92-98% (89-95%) of reactive (reflected) trajectories, dissociation (reflection) takes place after less than three rebounds, i.e.  $N_{\text{reb}} \leq 2$  (after only one rebound, i.e.  $N_{\text{reb}}=1$ ). Similar short interaction times and small number of rebounds have

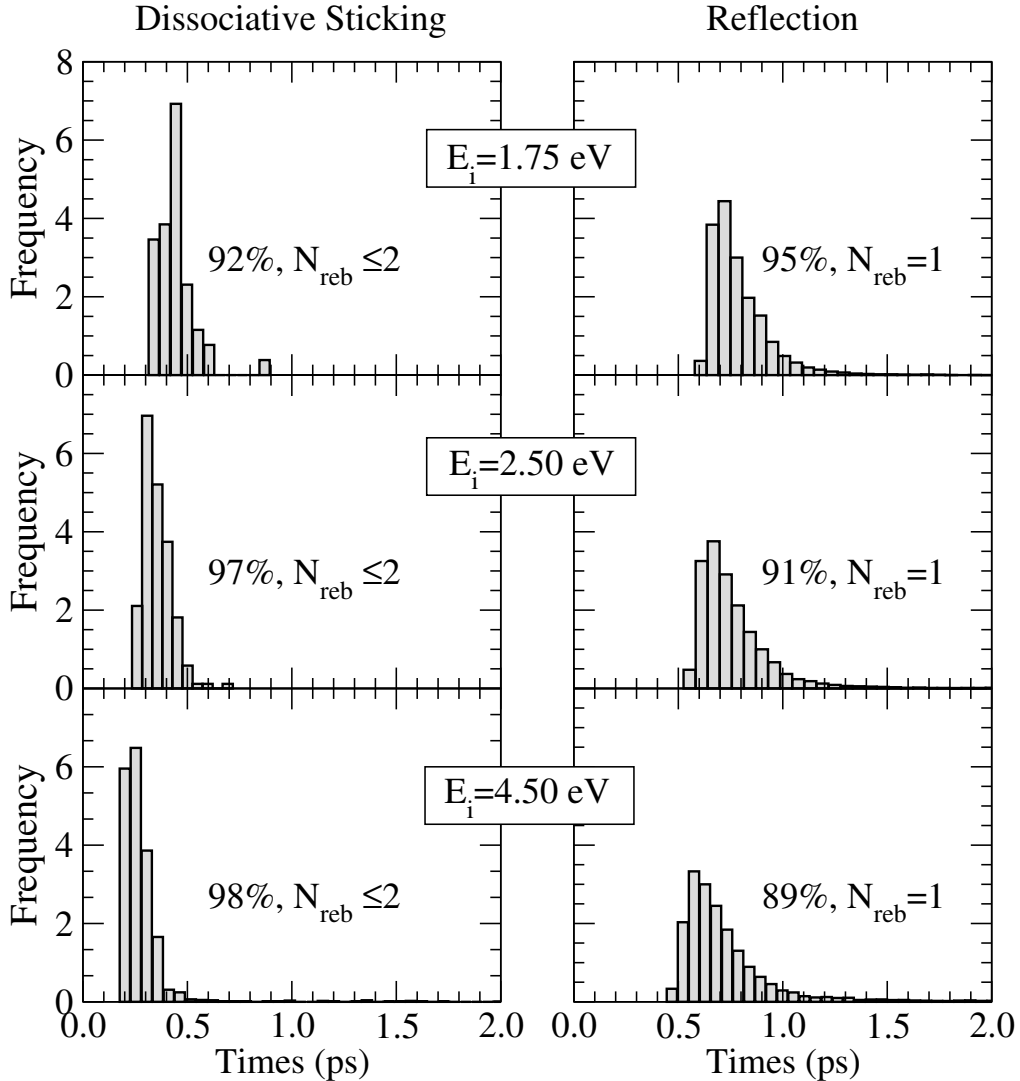


FIG. 8. Times for dissociative sticking (left panels) and reflection (right panels) of CO<sub>2</sub> molecules in a (6×6) supercell at  $T_s=300$  K. Three different values of the initial translational kinetic energy of the molecule are evaluated:  $E_i=1.75$  eV (upper panels),  $E_i=2.50$  eV (middle panels),  $E_i=4.50$  eV (lower panels).

also been found for  $E_i=1.25$  eV and 1.50 eV but in these cases, more trajectories would be needed to perform an analysis of the distribution of dissociation times with small statistical uncertainties and so, these energies have not been considered in Fig. 8. These results clearly show that for  $E_i \gtrsim 1.25$  eV for which we have found dissociative sticking events, the scattering of most molecules is direct no matter whether they reflect or dissociate on Cu(110).

In spite of the single-rebound character of reflection events for most molecules, they transfer a

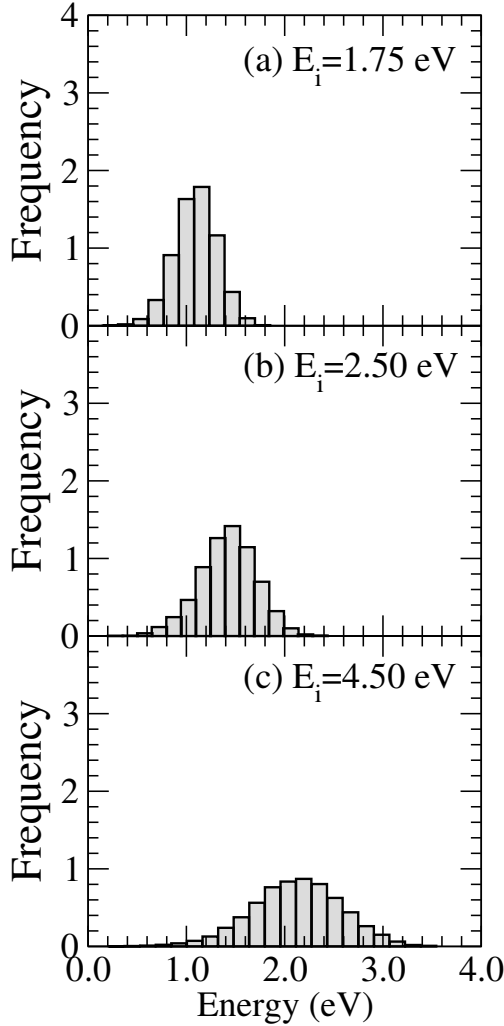


FIG. 9. Distribution of energy transferred by reflected CO<sub>2</sub> molecules to the Cu(110) surface at  $T_s = 300$  K for normal incidence. (a)  $E_i = 1.75$  eV, (b)  $E_i = 2.50$  eV, (c)  $E_i = 4.50$  eV.

significant fraction of the initial translational energy to the surface. Fig. 9 shows that for  $E_i = 1.75$  eV, 2.5 eV and 4.5 eV, reflected molecules transfer to the surface between 25% and 85% of their initial translational energy. Interestingly, even the upper bound of the energy transfer is smaller than the value predicted by the Baule formula<sup>63</sup>,  $\Delta E = 4\alpha E_i / (1 + \alpha)^2 \simeq 0.97 E_i$ , with  $\alpha \simeq 0.69$  being the ratio of the mass of a CO<sub>2</sub> molecule and the mass of a Cu atom.

In Fig. 10 we consider the influence of  $T_s$  on  $P_{\text{diss}}$  between 50 K and 400 K. Our calculations predict a negligible  $T_s$ -dependence in the whole range of  $E_i$  values considered, in line with experiments<sup>12,17</sup>. This is in contrast with activated dissociation of other molecule/surface systems (e.g. for CH<sub>4</sub> interacting with metal surfaces) for which  $P_{\text{diss}}$  strongly increases with  $T_s$ , in particular at low impact energies (see e.g. Ref. 64). Interestingly, allowing Cu atoms relaxation provoke

## CO<sub>2</sub> Dissociative Sticking on Cu(110)

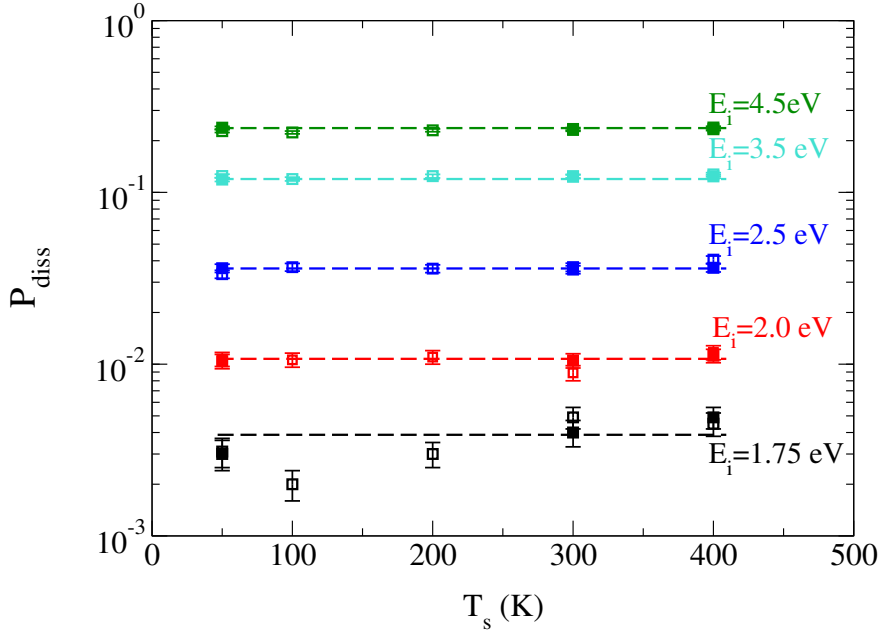


FIG. 10.  $P_{\text{diss}}$  as a function of surface temperature,  $T_s$ , for normal incidence and  $E_i$ : 1.75 eV (black), 2.0 eV (red), 2.5 eV (blue), 3.5 eV (turquoise), and 4.5 eV (dark green). Full symbols,  $(6 \times 6)$  supercell; open symbols,  $(3 \times 3)$  supercell. The dashed horizontal lines are plotted to guide the eyes.

a 0.15 eV reduction of the energy barrier for dissociation of CO<sub>2</sub> on Cu(110) (with respect to the value obtained within a rigid surface model) similar to what is found for various CH<sub>4</sub>/metal surface systems<sup>65</sup>. However, it must be noted that whereas the lattice distortion favorable for CH<sub>4</sub> activation simply consists in the shift up of its closest metal atom, in the case of CO<sub>2</sub>, appropriate concerted displacements of four neighbor Cu atoms with respect to their equilibrium positions are needed for the 0.15 eV energy-barrier reduction mentioned above. Therefore, the probability for a molecule to find a particular lattice distortion more convenient for dissociation simply induced by thermal fluctuations when  $T_s$  increases, is expected to be much smaller for CO<sub>2</sub> on Cu(110) than for CH<sub>4</sub> on metal surfaces. This provides a possible explanation of why surface temperature is not effective activating CO<sub>2</sub> in contrast with CH<sub>4</sub>.

Before concluding this section it is worth commenting that for  $E_i=1.5$  eV we have also performed calculations of  $P_{\text{diss}}$  for the CO<sub>2</sub> molecules initially in four vibrationally excited states: the first excited state of the asymmetric stretching (AS,  $v=1$ ), and symmetric stretching (SS,  $v=1$ ) modes, and the first and second excited state of the bending (B,  $v=1,2$ ) mode. According to our ANN-PES, the frequencies of these three vibrational modes of CO<sub>2</sub> in vacuum are: 2295 cm<sup>-1</sup> ( $\hbar\omega_{\text{AS}}=0.285$  eV), 1284 cm<sup>-1</sup> ( $\hbar\omega_{\text{SS}}=0.159$  eV), and 616 cm<sup>-1</sup> ( $\hbar\omega_{\text{B}}=0.076$  eV) respectively,

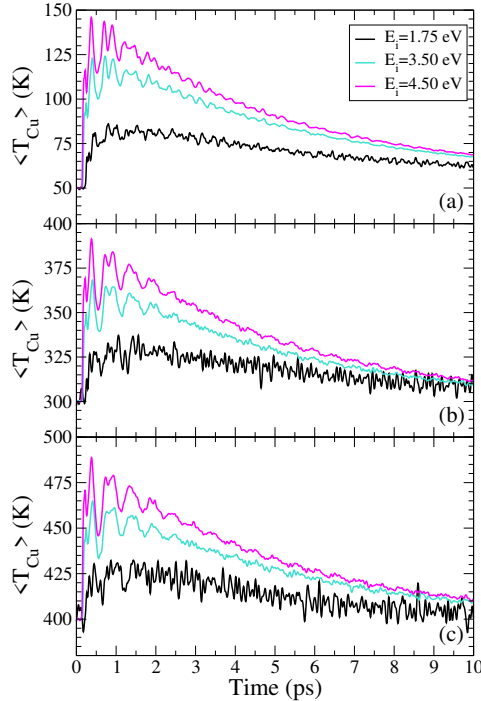


FIG. 11. Time evolution of the mean surface temperature  $\langle T_{\text{Cu}} \rangle$  for trajectories of dissociated molecules for  $E_i=1.75$  eV, 3.50 eV, and 4.5 eV, and initial surface temperatures: (a)  $T_s=50$  K, (b)  $T_s=300$  K, and (c)  $T_s=400$  K.

in good agreement with the experimental values. For all these excited states,  $P_{\text{diss}}$  is larger than for the ground state of CO<sub>2</sub>, by factors  $P_{\text{diss}}(\text{AS}, v=1)/P_{\text{diss}}(\text{GS})=4.1$ ,  $P_{\text{diss}}(\text{SS}, v=1)/P_{\text{diss}}(\text{GS})=2.5$ ,  $P_{\text{diss}}(\text{B}, v=2)/P_{\text{diss}}(\text{GS})=2.4$ , and  $P_{\text{diss}}(\text{B}, v=1)/P_{\text{diss}}(\text{GS})=1.8$ . The ordering of reactivity of these vibrationally excited states is consistent with that found by Yin and Guo<sup>16</sup>, and with the ordering of their internal energies. In particular, it is interesting to note that for the excited states SS,  $v=1$  and B,  $v=2$ , which have very similar total internal energies, the corresponding values of  $P_{\text{diss}}$  are also very close to each other, suggesting a small mode-specificity.

### 1. Final state of dissociation products

To characterize the final state of the dissociation products of CO<sub>2</sub>, for reactive trajectories we extended the integration time up to 10 ps. The choice of this integration time is justified by the temporal evolution of the average substrate temperature  $\langle T_{\text{Cu}} \rangle$  shown in Fig. 11. For three impact energies of CO<sub>2</sub> ranging from  $E_i=1.75$  eV to  $E_i=4.50$  eV, and for different initial surface temperatures:  $T_s=50$  K (a),  $T_s=300$  K (b), and  $T_s=400$  K (c),  $\langle T_{\text{Cu}} \rangle$  presents an abrupt increase

## CO<sub>2</sub> Dissociative Sticking on Cu(110)

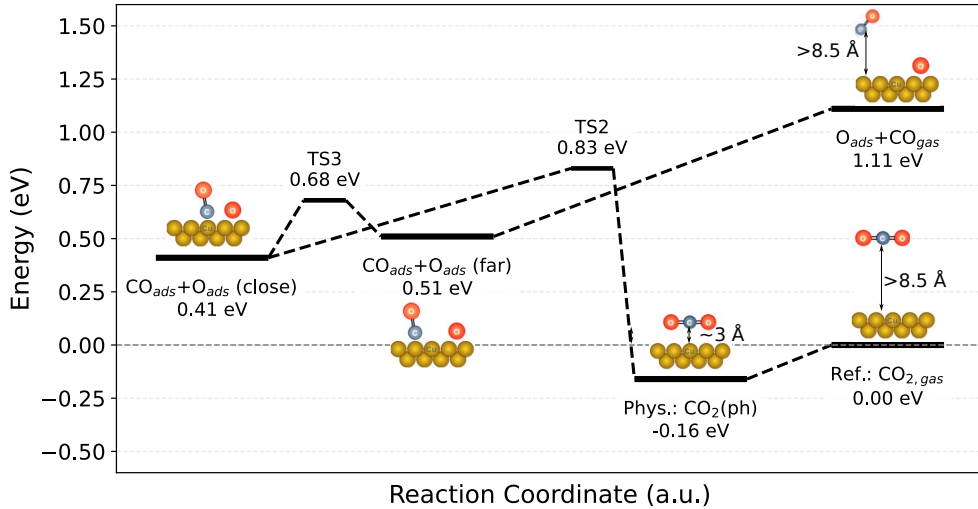


FIG. 12. Minimum energy pathways of various possible processes involving CO<sub>ads</sub> and O<sub>ads</sub> after CO<sub>2</sub> dissociation on Cu(110): diffusion of CO<sub>ads</sub> far from O<sub>ads</sub>, recombination to form CO<sub>2</sub> physisorbed or desorbed, and CO desorption.

at  $t \sim 0.2 - 0.3$  ps (more pronounced for higher impact energies) due to the energy transfer from the fast molecules to the surface. After this initial increase,  $\langle T_{\text{Cu}} \rangle$  gradually decays over time to reach at  $t_{\text{max}} = 10$  ps, a value similar to the initial  $T_s$ . Thus, an integration time of 10 ps ensures that most of the energy initially transferred to the substrate by the impinging molecule, has been dissipated.

Table I shows the percentage of the different final states of the CO<sub>2</sub> dissociation fragments on Cu(110), observed at  $t_{\text{max}} = 10$  ps for various initial molecular energies and surface temperatures. For the great majority of the trajectories, either CO and O both remain adsorbed on the surface (hereafter referred to as CO<sub>ads</sub>+O<sub>ads</sub> states) or only the O atom remains adsorbed whereas the CO molecule desorbs (hereafter referred to as CO<sub>gas</sub>+O<sub>ads</sub> states). The energetics of the most probable processes that can take place after dissociation starting from the lowest energy configuration with CO<sub>ads</sub> and O<sub>ads</sub> close to each other (characterized by a potential energy 0.41 eV) are summarized in Fig. 12. Recombination events leading to desorbed or physisorbed CO<sub>2</sub> molecules (i.e. CO<sub>2,gas</sub> or CO<sub>2,ph</sub> respectively) are very scarce. These final states have been found only for  $\sim 1\%$  of the dissociated molecules in the most favorable condition of high  $E_i$  and  $T_s$  values. Due to this reason, the percentage of recombination events for each initial condition ( $E_i, T_s$ ) have not been included in Tables I and II (see below).

## CO<sub>2</sub> Dissociative Sticking on Cu(110)

TABLE I. Percentage of different final states post-dissociation of CO<sub>2</sub> on Cu(110) at the final integration time  $t_{\max}=10$  ps, for  $T_s= 50, 300$ , and  $400$  K and  $E_i=1.75, 2.00, 2.50, 3.50$ , and  $4.50$  eV. The results correspond to calculations performed using a 6x6 supercell. The definition of each type of final states, is provided in the main text.

$E_i$ (eV)	CO <sub>gas</sub> +O <sub>ads</sub>	CO <sub>ads</sub> +O <sub>ads</sub>	+Cu-adatom
$T_s=50$ K			
<b>1.75</b>	0.00	100.00 (90.00)	0.00
<b>2.00</b>	0.96	95.19 (86.54)	3.85
<b>2.50</b>	8.84	87.56 (68.78)	3.59
<b>3.50</b>	31.20	60.89 (38.10)	7.23
<b>4.50</b>	55.84	30.88 (14.96)	12.36
$T_s=300$ K			
<b>1.75</b>	0.00	97.50 (85.00)	2.50
<b>2.00</b>	2.86	89.53 (75.24)	7.62
<b>2.50</b>	14.17	74.94 (51.23)	10.08
<b>3.50</b>	42.88	44.74 (22.25)	11.33
<b>4.50</b>	56.69	27.60 (10.42)	14.51
$T_s=400$ K			
<b>1.75</b>	2.04	81.63 (53.06)	16.33
<b>2.00</b>	3.54	76.39 (59.29)	19.46
<b>2.50</b>	16.30	66.03 (39.67)	16.58
<b>3.50</b>	40.53	39.09 (18.23)	19.02
<b>4.50</b>	56.15	21.79 (14.69)	19.72

The results reported in Table I show that CO<sub>ads</sub>+O<sub>ads</sub> is the dominant type of final dissociated states at the lowest impact energies considered, regardless of the value of  $T_s$ . When  $E_i$  and/or  $T_s$  increase, the percentage of CO<sub>ads</sub>+O<sub>ads</sub> (CO<sub>gas</sub>+O<sub>ads</sub>) final states decreases (increases) significantly. In the CO<sub>ads</sub>+O<sub>ads</sub> column of Table I, the first number indicates the total percentage of this type of final state whereas the second value (between parentheses) refers only to the cases in which both fragments remain within the same surface unit cell ( $|X_C - X_{O_{ads}}| \leq 2.654$  Å and

## CO<sub>2</sub> Dissociative Sticking on Cu(110)

$|Y_C - Y_{O_{ads}}| \leq 3.754 \text{ \AA}$ ). At low impact energies, the majority of the CO<sub>ads</sub> and O<sub>ads</sub> fragments remain close to each other within the same Cu(110) unit cell, but they end up farther apart from each other when  $E_i$  increases. For instance, for  $T_s=300$  K, 85% of dissociation products remain adsorbed close to each other for  $E_i=1.75$  eV but only  $\sim 10\%$  do it for  $E_i=4.5$  eV. This indicates that the initial translational energy of CO<sub>2</sub> does not dissipate efficiently before dissociation, being then transferred to a large extent, to the relative motion of the dissociation products.

The dissociation products of type CO<sub>ads</sub>+O<sub>ads</sub> that end far from each other after 10 ps are not likely to recombine and for  $T_s$  above  $\sim 200$  K (the desorption temperature of CO<sup>66–68</sup>), it is expected that most of them will eventually convert into CO<sub>gas</sub>+O<sub>ads</sub> due to CO thermal desorption. In contrast, one might argue that those CO<sub>ads</sub>+O<sub>ads</sub> dissociation products that after 10 ps are still close to each other might eventually recombine and desorb as CO<sub>2</sub>. This could approach the theoretical  $P_{diss}$  to experiments at high energies (see Fig. 6). However, this is not the case since for  $E_i=4.5$  eV and  $T_s=300$  K, only  $\sim 10\%$  of the CO<sub>ads</sub>+O<sub>ads</sub> dissociation products remain close to each other and even if all of them recombine, this would entail only a 10% reduction of  $P_{diss}$ .

It is important to mention that in the columns of Table I labeled as CO<sub>gas</sub>+O<sub>ads</sub> and CO<sub>ads</sub>+O<sub>ads</sub>, we have only considered final states of the dissociation products in which the surface structure is preserved. In contrast, in the right column of Table I labeled as *+Cu-adatom*, we report the total percentage of final states of the dissociation products that have been found coexisting with one Cu adatom located above the topmost-layer of the Cu(110) surface. The presence of Cu adatoms in the final state of each trajectory was evaluated considering the final height of each Cu atom with respect to the average height of the Cu atoms in the topmost-layer of Cu(110) in the initial configuration of the trajectory. We consider that a Cu atom is such an adatom when, at  $t_{max}=10$  ps, its Z coordinate,  $Z_{Cu} > \bar{Z}_{Cu-top}^{ini} + 0.5 d_{110}$ , being  $\bar{Z}_{Cu-top}^{ini}$  the average Z coordinate of all the topmost-layer Cu atoms in the initial state of the trajectory, and  $d_{110}$  the ideal (bulk-truncated) inter-layer distance between consecutive (110) crystallographic planes. Other types of lattice distortions have also been found in the final states of dissociation products but much less frequently than those with Cu adatoms, and so we will disregard them in what follows.

In Table I it is shown that the percentage of *+Cu-adatom* final states of dissociation products is negligible at low impact energies, increases with  $E_i$  and  $T_s$ , and reaches its maximum value  $\sim 20\%$  for  $E_i=4.5$  eV and  $T_s=400$  K. For final states of type *+Cu-adatom* we can also separate those configurations where both CO and O are adsorbed on the surface on one side, and those in which only the O atom remains adsorbed on the surface due to the desorption of CO on the other.

## CO<sub>2</sub> Dissociative Sticking on Cu(110)

These final states might also be referred to as CO<sub>ads</sub>+O<sub>ads</sub> and CO<sub>gas</sub>+O<sub>ads</sub> respectively as it was done before. However, to emphasize that now the structures involve one Cu adatom we introduce a new specific notation:

- **CO<sub>gas</sub>+(O<sub>ads</sub>+Cu)**: states in which CO is desorbed and the O atom remains adsorbed on the surface near (i.e. to a distance shorter than the length of the diagonal of the unit cell of Cu(110), 4.6 Å) or far from the Cu adatom,
- **CO<sub>ads</sub>+Cu+O<sub>ads</sub>**: states in which both CO and O are adsorbed on the surface being at most one of them close to the Cu adatom,
- **(O-Cu-CO)<sub>ads</sub>**: states in which both CO and O are adsorbed on the surface close to the Cu adatom, forming an almost linear O-Cu-CO chain moiety anchored to the surface through the O atom and being the Cu atom slightly detached from the surface.

In Table II we report the percentages of these three types of final states of dissociation products found in our calculations. In the case of CO<sub>gas</sub>+(O<sub>ads</sub>+Cu) we report the total percentage of this type of states, indicating between parentheses the percentage in which the O atom is close to the Cu adatom (i.e. to a distance shorter than 4.6 Å). It is observed that the percentage of this type of final state increases with the initial impact energy of the molecules. In most cases O<sub>ads</sub> is close to the Cu adatom suggesting that the O atom stabilizes or even assists the formation of the Cu adatom. The energetics of the creation of a single Cu adatom (predicted by our ANN-PES) for different relative distances between O<sub>ads</sub> and CO<sub>ads</sub> from the Cu adatom is shown in Fig. 13. It can be observed that the energy cost and the barrier for the formation of a single Cu adatom with no influence of CO<sub>ads</sub> and O<sub>ads</sub> are 0.51 eV and 0.58 eV (TS6) respectively. In contrast, if O<sub>ads</sub> is close to the Cu adatom these values reduce to 0.71 eV - 0.53 eV = 0.18 eV and 0.87 eV - 0.53 eV = 0.34 eV (TS8) respectively. This is consistent with the fact that in most of the final structures CO<sub>gas</sub>+(O<sub>ads</sub>+Cu), the O<sub>ads</sub> species is close to the Cu adatom.

In the column labeled as CO<sub>ads</sub>+Cu+O<sub>ads</sub> we report the total percentage of this type of final dissociated states followed by two numbers between parentheses, corresponding to (from left to right) configurations with CO<sub>ads</sub> close to (and O<sub>ads</sub> far from) the Cu adatom, and O<sub>ads</sub> close to (and CO<sub>ads</sub> far from) the Cu adatom. Here, we have considered that a dissociation product (CO<sub>ads</sub> or O<sub>ads</sub>) is close to (far from) a Cu adatom when it is located a distance  $\leq$  4.6 Å ( $\geq$  4.6 Å) to it. First, as expected, total percentage of this type of final states involving a Cu adatom increases with

## CO<sub>2</sub> Dissociative Sticking on Cu(110)

TABLE II. Classification of final-state channels involving Cu atoms that have shifted up with respect to the topmost layer of the slab, resulting from CO<sub>2</sub> dissociation on a 6×6-Cu(110) cell, for T<sub>s</sub>=50 K, 300 K, and 400 K. A detailed description of each configuration is provided in the main text.

E <sub>i</sub> (eV)	CO <sub>gas</sub> +(O <sub>ads</sub> + Cu)	CO <sub>ads</sub> + Cu + O <sub>ads</sub>	(O-Cu-CO) <sub>ads</sub>
T <sub>s</sub> =50 K			
<b>1.75</b>	0.00 (0.00)	0.00 (0.00, 0.00 )	0.00
<b>2.00</b>	0.00 (0.00)	0.00 (0.00, 0.00)	3.85
<b>2.50</b>	0.28 (0.28)	0.28 (0.00, 0.28)	3.04
<b>3.50</b>	1.60 (1.60)	2.86 (0.93, 1.60)	2.78
<b>4.50</b>	6.05 (5.97)	4.00 (1.01, 2.82)	2.27
T <sub>s</sub> =300 K			
<b>1.75</b>	0.00 (0.00)	0.00 (0.00, 0.00)	2.50
<b>2.00</b>	0.00 (0.00)	1.90 (1.90, 0.00)	5.71
<b>2.50</b>	0.27 (0.27)	2.99 (1.09, 0.82 )	6.81
<b>3.50</b>	2.51 (1.94)	4.12 (1.78, 1.29)	4.61
<b>4.50</b>	5.68 (4.34)	5.83 (1.77, 2.68)	2.92
T <sub>s</sub> =400 K			
<b>1.75</b>	0.00 (0.00)	10.20 (10.20, 0.00 )	6.12
<b>2.00</b>	0.00 (0.00)	11.49 (7.96, 0.88 )	7.96
<b>2.50</b>	0.82 (0.27)	9.51 (4.62, 3.26 )	6.25
<b>3.50</b>	3.43 (2.48)	8.88 (3.52, 2.64 )	6.63
<b>4.50</b>	7.67 (5.03)	7.84 (2.60, 2.64 )	4.17

surface temperature. In addition, in most of CO<sub>ads</sub>+Cu+O<sub>ads</sub> final states, either CO<sub>ads</sub> or O<sub>ads</sub> are close to the Cu adatom which indicates that the presence of CO<sub>ads</sub> also stabilizes and/or assists the formation of Cu adatoms. This is confirmed by Fig. 13 where we show that if CO<sub>ads</sub> is close to the Cu adatom the energy cost and barrier for formation of a Cu adatom are 0.80 eV - 0.53 eV = 0.27 eV and 0.89 eV - 0.53 eV = 0.36 eV (TS7) (to be compared with 0.51 eV and 0.58 eV for the *non-adsorbate-assisted* creation of a Cu adatom) respectively. Moreover, it is important to mention that in most of the final states with CO<sub>ads</sub> close to the Cu adatom, the molecule is directly

## CO<sub>2</sub> Dissociative Sticking on Cu(110)

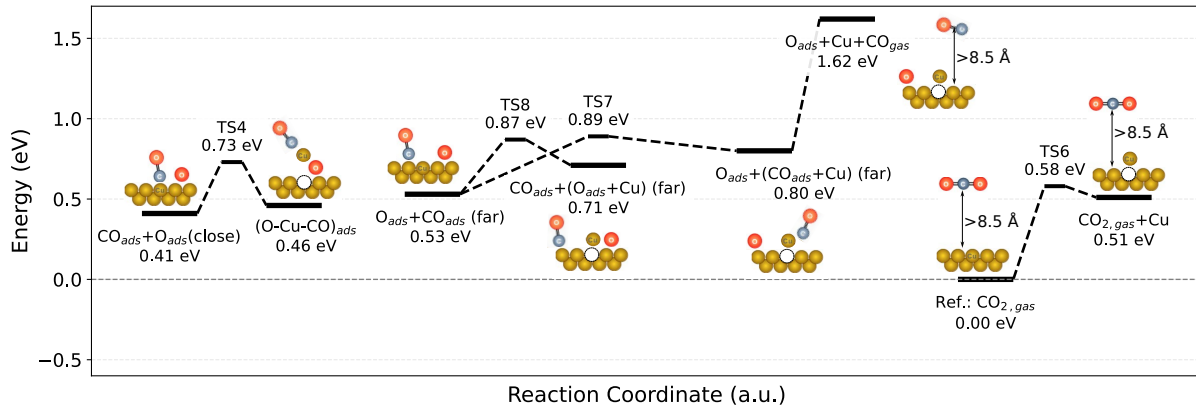


FIG. 13. Minimum energy pathways of various possible processes involving CO<sub>ads</sub> and O<sub>ads</sub> after CO<sub>2</sub> dissociation on Cu(110), in presence of and/or inducing Cu adatom-vacancy pair formation.

chemisorbed on top of it, the desorption energy from this state being 0.82 eV, i.e. 0.22 eV higher than the desorption energy of CO from Cu(110) with no adatoms.

Finally, the percentage of (O-Cu-CO)<sub>ads</sub> final states also increases with surface temperature. The energy of this final state is only 0.05 eV higher than the most stable final dissociated state with CO<sub>ads</sub> and O<sub>ads</sub> chemisorbed within the same unit cell of Cu(110) and the energy barrier for the creation of this linear O-Cu-CO chain moiety (TS4) is only 0.73 eV - 0.41 eV = 0.32 eV (Fig. 13). This explains the relatively large probabilities of this unexpected final state in which a Cu adatom looks detached from the surface and forming a O-Cu-CO chain anchored to the surface through the dissociated O atom. It might be argued that this final state might be simply a consequence of an artifact of the ANN-PES used in the QCT calculations. However, it is not the case. It must be emphasized that some of this kind of (O-Cu-CO)<sub>ads</sub> structures are included in the data base used for training of the ANN-PES during the active learning procedure employed. The MAE of the ANN-PES for a sub-set of 25 of these configurations is only 1.9 meV/atom. This highlights the importance of using the active learning method that allows unexpected configurations visited by the trajectories during the simulations (that would be otherwise overlooked), to be identified and incorporated into the training database.

#### IV. CONCLUSIONS

In this work we have used quasi-classical trajectory calculations to investigate the dynamics of CO<sub>2</sub> molecular and dissociative adsorption on Cu(110) as a function of the initial translational energy of the molecule,  $E_i$ , and surface temperature,  $T_s$ . These calculations were performed by using an artificial neural network (ANN) potential energy surface (PES) optimized in this work for the CO<sub>2</sub>/Cu(110) system, through an iterative active learning approach, to properly describe density functional theory (DFT) total energies for a large set of system configurations. By using the vdW-DF2 exchange-correlation functional, we obtained that the global energy minimum of the system corresponds to weakly bound CO<sub>2</sub> physisorbed on Cu(110) with energy  $\sim 0.17$  eV below the lowest value obtained for the molecule far from the surface that we take as our zero-energy reference level. We have also found chemisorbed bent state with energy +0.49 eV, which is highly unstable because an energy barrier of only +0.01 eV is found along the minimum energy path (MEP) connecting this local minimum with the global minimum of the PES. In addition, the energy of the transition state found along the MEP connecting the physisorbed state and the most stable dissociated state (of energy +0.41 eV) corresponding to both CO and O adsorbed within the same surface unit cell is +0.83 eV.

We have found that physisorption is the dominant adsorption channel below the desorption temperature of CO<sub>2</sub> (i.e.  $T_s \sim 90$  K) and for  $E_i$  up to  $\sim 1.75$  eV also in qualitative agreement with experiments but the initial decrease of the corresponding  $P_{\text{molads}}(E_i)$  theoretical curve is much more pronounced than in experiments. The dissociation probability presents a monotonic increasing  $E_i$ -dependence with a decreasing slope of the  $P_{\text{diss}}(E_i)$  curve in agreement with experiments. However, the agreement with supersonic molecular beam experiments is only qualitative since our results underestimate the experimental values for  $E_i \lesssim 2$  eV and overestimate them for  $E_i \gtrsim 2$  eV.

Also in agreement with experiments, we have found that  $P_{\text{diss}}$  is not affected by surface temperature between 50 K and 400 K. Interestingly, this is in spite of a non-negligible reduction of the energy barrier for CO<sub>2</sub> when Cu atoms are allowed to adapt their optimum positions in presence of the molecule. This negligible  $T_s$ -sensitivity is attributed to the fact that concerted particularly appropriate displacements of various neighboring Cu atoms is required to significantly reduce the energy of the CO<sub>2</sub> transition state for dissociation. Therefore, the probability of inducing such a particular set of Cu-displacements thanks to thermal fluctuations by increasing surface temperature, in order to offer to the incoming (fast) molecules more favorable dissociation pathways is

## CO<sub>2</sub> Dissociative Sticking on Cu(110)

very small.

We have also characterized the final state of the dissociation products, the most probable one being CO<sub>ads</sub>+O<sub>ads</sub> (both species adsorbed) at low energies and CO<sub>gas</sub>+O<sub>ads</sub> (only O adsorbed and CO desorbed) at higher energies. However, above 200 K (the desorption temperature of CO from Cu(110)) it is expected that the CO<sub>ads</sub> species found in simulations would eventually desorb at longer times, remaining at the end only oxygen atoms adsorbed on the surface in agreement with experiments performed for instance at room temperature (RT). Interestingly, we have found that for molecules with impact energies above  $\sim 2.5$  eV (in particular for RT and above), dissociation events produce with a non-negligible probability, surface distortions involving Cu adatoms. The presence of the CO and O adsorbed species reduce the energy barrier for creation of Cu adatoms which in turn can be overcome more easily by the system for high impact energy molecules due to a relatively efficient energy transfer to lattice vibrations. The changes observed at  $E_i \sim 2.5$  eV, in the final state of dissociation products from the case of low to high energy molecules might provide a possible explanation for the experiments that have found that the saturation atomic oxygen coverage achieved for CO<sub>2</sub> with impact energies larger than 3 eV (0.66 ML) is larger than for lower energy molecules (0.50 ML). Still, additional experimental and also theoretical investigations are needed to fully elucidate the origin of the latter so far unexplained experimental results.

## ACKNOWLEDGMENTS

This work has been supported by the ANPCyT Project PICT-2021-I-A-01135, CONICET Project PIP 1679, and the UNR Project PID 80020190100011UR (Argentina). The authors acknowledge computer time provided by CCT-Rosario Computational Center, member of the High Performance Computing National System of Argentina (SNCAD).

## AUTHOR CONTRIBUTIONS

All the authors participated in the calculations, analysis and discussion of the results, and writing of the manuscript.

## DATA AVAILABILITY STATEMENT

The data that support the findings of this study are available from the corresponding author upon reasonable request.

## CONFLICTS OF INTEREST

The authors have no conflicts to disclose.

## REFERENCES

<sup>1</sup>M. Gattrell, N. Gupta, and A. Co. A review of the aqueous electrochemical reduction of CO<sub>2</sub> to hydrocarbons at copper. *Journal of Electroanalytical Chemistry*, 594(1):1–19, 2006.

<sup>2</sup>Evgenii V. Kondratenko, Guido Mul, Jonas Baltrusaitis, Gastón O. Larrazábal, and Javier Pérez-Ramírez. Status and perspectives of CO<sub>2</sub> conversion into fuels and chemicals by catalytic, photocatalytic and electrocatalytic processes. *Energy & Environmental Science*, 6(11):3112, 2013.

<sup>3</sup>Juntian Niu, Haiyu Liu, Yan Jin, Baoguo Fan, Wenjie Qi, and Jingyu Ran. Comprehensive review of Cu-based CO<sub>2</sub> hydrogenation to CH<sub>3</sub>OH: Insights from experimental work and theoretical analysis. *International Journal of Hydrogen Energy*, 47(15):9183–9200, 2022.

<sup>4</sup>Xiaorong Zhu and Yafei Li. Review of two-dimensional materials for electrochemical CO<sub>2</sub> reduction from a theoretical perspective. *WIREs Computational Molecular Science*, 9(6):e1416, 2019.

<sup>5</sup>Steven R. Kass. Carbon dioxide stability and C=O  $\pi$ -bond strengths. *The Journal of Organic Chemistry*, 89(16):11353–11356, 2024. PMID: 39107977.

<sup>6</sup>Shyam Kattel, Ping Liu, and Jingguang G. Chen. Tuning selectivity of CO<sub>2</sub> hydrogenation reactions at the metal/oxide interface. *Journal of the American Chemical Society*, 139(29):9739–9754, 2017.

<sup>7</sup>Hilmar Guzmán, Fabio Salomone, Samir Bensaid, Micaela Castellino, Nunzio Russo, and Simelys Hernández. CO<sub>2</sub> conversion to alcohols over Cu/ZnO catalysts: Prospective synergies between electrocatalytic and thermocatalytic routes. *ACS Applied Materials & Interfaces*, 14(1):517–530, 2022. PMID: 34965095.

## CO<sub>2</sub> Dissociative Sticking on Cu(110)

<sup>8</sup>Gui-Chang Wang, Ling Jiang, Yoshitada Morikawa, Junji Nakamura, Zun-Sheng Cai, Yin-Ming Pan, and Xue-Zhuang Zhao. Cluster and periodic dft calculations of adsorption and activation of CO<sub>2</sub> on the Cu(hkl) surfaces. *Surface Science*, 570(3):205–217, 2004.

<sup>9</sup>J Nakamura, J A Rodriguez, and C T Campbell. Does CO<sub>2</sub> dissociatively adsorb on Cu surfaces? *Journal of Physics: Condensed Matter*, 1(SB):SB149–SB160, October 1989.

<sup>10</sup>Sabrina S. Fu and Gabor A. Somorjai. Interactions of O<sub>2</sub>, CO, CO<sub>2</sub>, and D<sub>2</sub> with the stepped Cu(311) crystal face: Comparison to Cu(110). *Surface Science*, 262(1–2):68–76, February 1992.

<sup>11</sup>S. Funk, B. Hokkanen, J. Wang, U. Burghaus, G. Bozzolo, and J.E. Garcés. Adsorption dynamics of CO<sub>2</sub> on Cu(110): A molecular beam study. *Surface Science*, 600(3):583–590, 2006.

<sup>12</sup>Saurabh Kumar Singh and Pranav R. Shirhatti. The curious case of CO<sub>2</sub> dissociation on Cu(110). *The Journal of Chemical Physics*, 160(2):024702, 01 2024.

<sup>13</sup>Gui-Chang Wang, Ling Jiang, Xian-Yong Pang, Zun-Sheng Cai, Yin-Ming Pan, Xue-Zhuang Zhao, Yoshitada Morikawa, and Junji Nakamura. A theoretical study of surface-structural sensitivity of the reverse water-gas shift reaction over Cu(hkl) surfaces. *Surface Science*, 543(1):118–130, 2003.

<sup>14</sup>Tian Yang, Tangjie Gu, Yong Han, Weijia Wang, Yi Yu, Yijing Zang, Hui Zhang, Baohua Mao, Yimin Li, Bo Yang, and Zhi Liu. Surface orientation and pressure dependence of CO<sub>2</sub> activation on Cu surfaces. *The Journal of Physical Chemistry C*, 124(50):27511–27518, 2020.

<sup>15</sup>Jiří Klimeš, David R Bowler, and Angelos Michaelides. Chemical accuracy for the van der waals density functional. *Journal of Physics: Condensed Matter*, 22(2):022201, dec 2009.

<sup>16</sup>Rongrong Yin and Hua Guo. Multidimensional dynamics of CO<sub>2</sub> dissociative chemisorption on Cu(110). *The Journal of Physical Chemistry C*, 128(23):9483–9491, 2024.

<sup>17</sup>Saurabh Kumar Singh and Pranav R. Shirhatti. Dissociation dynamics of CO<sub>2</sub> on Cu(110) studied over a wide range of incident energies. *The Journal of Physical Chemistry C*, 128(49):20841–20848, 2024.

<sup>18</sup>Kyuho Lee, Éamonn D. Murray, Lingzhu Kong, Bengt I. Lundqvist, and David C. Langreth. Higher-accuracy van der waals density functional. *Phys. Rev. B*, 82:081101, Aug 2010.

<sup>19</sup>Federico J. Gonzalez, Giulia N. Seminara, Miranda I. López, Juan M. Lombardi, Maximiliano Ramos, Carmen A. Tachino, Alejandra E. Martínez, and H. Fabio Busnengo. Assessing the dynamics of CO adsorption on Cu(110) using the vdW-DF2 functional and artificial neural networks. *J. Chem. Phys.*, 159(22):224709, 12 2023.

<sup>20</sup>Federico J. Gonzalez, Alberto S. Muzas, J. Iñaki Juaristi, Maite Alducin, and H. Fabio Busnengo. Femtosecond laser-induced diffusion and desorption of CO adsorbed on a weak electron–phonon coupling surface: Cu(110). *The Journal of Chemical Physics*, 162(17):174701, 05 2025.

<sup>21</sup>G. Kresse and J. Hafner. *Ab initio* molecular dynamics for liquid metals. *Phys. Rev. B*, 47:558–561, Jan 1993.

<sup>22</sup>G. Kresse and J. Hafner. Ab initio molecular-dynamics simulation of the liquid-metal–amorphous-semiconductor transition in germanium. *Phys. Rev. B*, 49:14251–14269, May 1994.

<sup>23</sup>G Kresse and J Hafner. Norm-conserving and ultrasoft pseudopotentials for first-row and transition elements. *J. Phys.: Condens. Matt.*, 6(40):8245–8257, October 1994.

<sup>24</sup>G. Kresse and J. Furthmüller. Efficiency of ab-initio total energy calculations for metals and semiconductors using a plane-wave basis set. *Comput. Mater. Sci.*, 6(1):15 – 50, 1996.

<sup>25</sup>G. Kresse and J. Furthmüller. Efficient iterative schemes for ab initio total-energy calculations using a plane-wave basis set. *Phys. Rev. B*, 54:11169–11186, Oct 1996.

<sup>26</sup>G. Kresse and D. Joubert. From ultrasoft pseudopotentials to the projector augmented-wave method. *Phys. Rev. B*, 59:1758–1775, Jan 1999.

<sup>27</sup>P. E. Blöchl. Projector augmented-wave method. *Phys. Rev. B*, 50:17953–17979, Dec 1994.

<sup>28</sup>M. Methfessel and A. T. Paxton. High-precision sampling for brillouin-zone integration in metals. *Phys. Rev. B*, 40:3616–3621, Aug 1989.

<sup>29</sup>Hendrik J. Monkhorst and James D. Pack. Special points for brillouin-zone integrations. *Phys. Rev. B*, 13:5188–5192, Jun 1976.

<sup>30</sup>Greg Mills and Hannes Jónsson. Quantum and thermal effects in h<sub>2</sub> dissociative adsorption: Evaluation of free energy barriers in multidimensional quantum systems. *Phys. Rev. Lett.*, 72:1124–1127, Feb 1994.

<sup>31</sup>Gregory Mills, Hannes Jónsson, and Gregory K. Schenter. Reversible work transition state theory: application to dissociative adsorption of hydrogen. *Surf. Sci.*, 324(2–3):305 – 337, 1995.

<sup>32</sup>H. Jónsson, G. Mills, and K. W. Jacobsen. *Nudged elastic band method for finding minimum energy paths of transitions*. In *Classical and Quantum Dynamics in Condensed Phase Simulations*, edited by B. J. Berne and G. Ciccotti and D. F. Coker. World Scientific, Singapore, 1998.

<sup>33</sup>Graeme Henkelman and Hannes Jónsson. A dimer method for finding saddle points on high dimensional potential surfaces using only first derivatives. *The Journal of Chemical Physics*, 111(15):7010–7022, 10 1999.

<sup>34</sup>Nongnuch Artrith and Alexander Urban. An implementation of artificial neural-network potentials for atomistic materials simulations: Performance for  $\text{tio}_2$ . *Computational Materials Science*, 114:135–150, 2016.

<sup>35</sup>Nongnuch Artrith, Alexander Urban, and Gerbrand Ceder. Efficient and accurate machine-learning interpolation of atomic energies in compositions with many species. *Phys. Rev. B*, 96:014112, Jul 2017.

<sup>36</sup>April M. Cooper, Johannes Kästner, Alexander Urban, and Nongnuch Artrith. Efficient training of ann potentials by including atomic forces via taylor expansion and application to water and a transition-metal oxide. *npj Computational Materials*, 6, 2020.

<sup>37</sup>Jörg Behler. First principles neural network potentials for reactive simulations of large molecular and condensed systems. *Angew. Chem. Int. Ed.*, 56(42):12828–12840, 2017.

<sup>38</sup>Graeme Henkelman and Hannes Jónsson. Improved tangent estimate in the nudged elastic band method for finding minimum energy paths and saddle points. *J. Chem. Phys.*, 113(22):9978–9985, 12 2000.

<sup>39</sup>Graeme Henkelman, Blas P. Uberuaga, and Hannes Jónsson. A climbing image nudged elastic band method for finding saddle points and minimum energy paths. *J. Chem. Phys.*, 113(22):9901–9904, 12 2000.

<sup>40</sup>Søren Smidstrup, Andreas Pedersen, Kurt Stokbro, and Hannes Jónsson. Improved initial guess for minimum energy path calculations. *J. Chem. Phys.*, 140(21):214106, 06 2014.

<sup>41</sup>Esben L. Kolsbjer, Michael N. Groves, and Bjørk Hammer. An automated nudged elastic band method. *J. Chem. Phys.*, 145(9):094107, 09 2016.

<sup>42</sup>Stela Makri, Christoph Ortner, and James R. Kermode. A preconditioning scheme for minimum energy path finding methods. *J. Chem. Phys.*, 150(9):094109, 03 2019.

<sup>43</sup>S. R. Bahn and K. W. Jacobsen. An object-oriented scripting interface to a legacy electronic structure code. *Comput. Sci. Eng.*, 4(3):56–66, MAY-JUN 2002.

<sup>44</sup>Ask Hjorth Larsen, Jens Jørgen Mortensen, Jakob Blomqvist, Ivano E Castelli, Rune Christensen, Marcin Dułak, Jesper Friis, Michael N Groves, Bjørk Hammer, Cory Hargus, Eric D Hermes, Paul C Jennings, Peter Bjerre Jensen, James Kermode, John R Kitchin, Esben Leonhard Kolsbjer, Joseph Kubal, Kristen Kaasbjer, Steen Lysgaard, Jón Bergmann Maronsson, Tristan Maxson, Thomas Olsen, Lars Pastewka, Andrew Peterson, Carsten Rostgaard, Jakob Schiøtz, Ole Schütt, Mikkel Strange, Kristian S Thygesen, Tejs Vegge, Lasse Vilhelmsen, Michael Walter, Zhenhua Zeng, and Karsten W Jacobsen. The atomic simulation environment—a python

library for working with atoms. *J. Condens. Matter Phys.*, 29(27):273002, 2017.

<sup>45</sup>X. J. Shen, A. Lozano, W. Dong, H. F. Busnengo, and X. H. Yan. Towards bond selective chemistry from first principles: Methane on metal surfaces. *Phys. Rev. Lett.*, 112:046101, Jan 2014.

<sup>46</sup>A. Lozano, X.J. Shen, R. Moiraghi, W. Dong, and H.F. Busnengo. Cutting a chemical bond with demon's scissors: Mode- and bond-selective reactivity of methane on metal surfaces. *Surf. Sci.*, 640:25 – 35, 2015. Reactivity Concepts at Surfaces: Coupling Theory with Experiment.

<sup>47</sup>Giulia N. Seminara, Iván F. Peludhero, Wei Dong, Alejandra E. Martínez, and H. Fabio Busnengo. Molecular dynamics study of molecular and dissociative adsorption using system-specific force fields based on ab initio calculations: Co/cu(110) and ch<sub>4</sub>/pt(110). *Topics in Catalysis*, 62(12):1044 – 1052, 2019.

<sup>48</sup>Raquel Moiraghi, Ariel Lozano, Eric Peterson, Arthur Utz, Wei Dong, and H. Fabio Busnengo. Nonthermalized precursor-mediated dissociative chemisorption at high catalysis temperatures. *J. Phys. Chem. Lett.*, 11(6):2211–2218, 2020.

<sup>49</sup>I. F. Peludhero, A. Gutiérrez-González, W. Dong, R. D. Beck, and H. F. Busnengo. Dissociative sticking probability of methane on pt(110)-(2×1). *J. Phys. Chem. C.*, 125(22):11904–11915, 2021.

<sup>50</sup>Alejandro Rivero Santamaría, Maximiliano Ramos, Maite Alducin, Heriberto Fabio Busnengo, Ricardo Díez Muiño, and J. Iñaki Juaristi. High-dimensional atomistic neural network potential to study the alignment-resolved o<sub>2</sub> scattering from highly oriented pyrolytic graphite. *J. Phys. Chem. A.*, 125(12):2588–2600, 2021.

<sup>51</sup>P. Schofield. Computer simulation studies of the liquid state. *Comput. Phys. Commun.*, 5(1):17–23, 1973.

<sup>52</sup>Loup Verlet. Computer "experiments" on classical fluids. i. thermodynamical properties of lennard-jones molecules. *Phys. Rev.*, 159:98–103, Jul 1967.

<sup>53</sup>Loup Verlet. Computer "experiments" on classical fluids. ii. equilibrium correlation functions. *Phys. Rev.*, 165:201–214, Jan 1968.

<sup>54</sup>H. J. C. Berendsen, J. P. M. Postma, W. F. van Gunsteren, A. DiNola, and J. R. Haak. Molecular dynamics with coupling to an external bath. *J. Chem. Phys.*, 81(8):3684–3690, 10 1984.

<sup>55</sup>Thomas D. Sewell and Donald L. Thompson. Classical trajectory methods for polyatomic molecules. *Int. J. Mod. Phys. B*, 11(09):1067–1112, 1997.

<sup>56</sup>J. D. Hunter. Matplotlib: A 2d graphics environment. *Comput. Sci. Eng.*, 9(3):90–95, 2007.

## CO<sub>2</sub> Dissociative Sticking on Cu(110)

<sup>57</sup>Fahdzi Muttaqien, Yuji Hamamoto, Ikutaro Hamada, Kouji Inagaki, Yuichiro Shiozawa, Kozo Mukai, Takanori Koitaya, Shinya Yoshimoto, Jun Yoshinobu, and Yoshitada Morikawa. CO<sub>2</sub> adsorption on the copper surfaces: van der Waals density functional and TPD studies. *J. Chem. Phys.*, 147(9):094702, 09 2017.

<sup>58</sup>Karl-Heinz Ernst, Dirk Schlatterbeck, and Klaus Christmann. Adsorption of carbon dioxide on cu(110) and on hydrogen and oxygen covered cu(110) surfaces. *Physical Chemistry Chemical Physics*, 1:4105–4112, 1999.

<sup>59</sup>Michael D. Higham, Matthew G. Quesne, and C. Richard A. Catlow. Mechanism of co<sub>2</sub> conversion to methanol over cu(110) and cu(100) surfaces. *Dalton Transactions*, 49(25):8478–8497, 2020.

<sup>60</sup>Ubong J. Etim, Chenchen Zhang, and Ziyi Zhong. Impacts of the catalyst structures on co<sub>2</sub> activation on catalyst surfaces. *Nanomaterials*, 11(12):3265, November 2021.

<sup>61</sup>Bret Jackson. Direct and trapping-mediated pathways to dissociative chemisorption: CH<sub>4</sub> dissociation on ir(111) with step defects. *The Journal of Chemical Physics*, 153(3):034704, 07 2020.

<sup>62</sup>Xueyao Zhou, Yaolong Zhang, Hua Guo, and Bin Jiang. Towards bridging the structure gap in heterogeneous catalysis: the impact of defects in dissociative chemisorption of methane on ir surfaces. *Phys. Chem. Chem. Phys.*, 23:4376–4385, 2021.

<sup>63</sup>J. Harris. in dynamics of gas-surface interactions (eds: Rettner c. t., ashfold m. n. r.). pages 6–46, 1991.

<sup>64</sup>Bret Jackson. The effects of lattice motion on gas-surface reactions. In Ricardo Díez Muiño and Heriberto Fabio Busnengo, editors, *Dynamics of Gas-Surface Interactions*, volume 50 of *Springer Series in Surface Sciences*, chapter 9, pages 213–237. Springer Berlin Heidelberg, 2013.

<sup>65</sup>Sven Nave, Ashwani Kumar Tiwari, and Bret Jackson. Methane dissociation and adsorption on ni(111), pt(111), ni(100), pt(100), and pt(110)-(1×2): Energetic study. *J. Chem. Phys.*, 132(5):054705, 2010.

<sup>66</sup>K Horn, M Hussain, and J Pritchard. The adsorption of co on cu(110). *Surf. Sci.*, 63:244–253, 1977.

<sup>67</sup>M. Christiansen, E.V. Thomsen, and J. Onsgaard. Coadsorption of k and co on cu(110). *Surf. Sci.*, 261(1):179–190, 1992.

## CO<sub>2</sub> Dissociative Sticking on Cu(110)

<sup>68</sup>Joachim Ahner, Dan Mocuta, R. D. Ramsier, and John T. Yates. Adsorbate–adsorbate repulsions—the coverage dependence of the adsorption structure of co on cu(110) as studied by electron-stimulated desorption ion angular distribution. *J. Chem. Phys.*, 105(15):6553–6559, 1996.